NE contribution to rebooting unconsciousness caused by midazolam

LeYuan Gu[1,2#], WeiHui Shao[2#], Lu Liu[1#], Qing Xu[1#], YuLing Wang[2#], JiaXuan Gu[2#], Yue Yang[2], ZhuoYue Zhang[1], YaXuan Wu[2], Yue Shen[3], Qian Yu[2], XiTing Lian[1], Haixiang Ma[5], YuanLi Zhang[2], HongHai Zhang[1,2,3,4]*

[1]Department of Anesthesiology, Zhejiang University School of Medicine, Hangzhou, 310006, China

[2]Department of Anesthesiology, the Fourth Clinical School of Medicine, Zhejiang Chinese Medical University, Hangzhou, 310006, China

[3]Department of Anesthesiology, Affiliated Hangzhou First People's Hospital, Westlake University School of Medicine, Hangzhou, 310006, China

[4]Westlake Laboratory of Life Sciences and Biomedicine, Hangzhou, 310006, China

[5]Medical College of Jining Medical University, Ningji, 272067, Shandong, China

[#]These authors contributed equally to this work

Corresponding authors: HongHai Zhang

Email address: zhanghonghai_0902@163.com & zhh0902@zju.edu.cn

ORCID: http://orcid.org/0000-0003-3530-2060

Abstract

The advent of midazolam holds profound implications for modern clinical practice. The hypnotic and sedative effects of midazolam afford it broad clinical applicability. However, the specific mechanisms underlying the modulation of altered consciousness by midazolam remain elusive. Herein, using pharmacology, optogenetics, chemogenetics, fiber photometry, and gene knockdown, we revealed the role of locus coeruleus (LC)-ventrolateral preoptic nucleus (VLPO) noradrenergic neural circuit in regulating midazolam-induced altered consciousness. This effect was mediated by α1 adrenergic receptors. Moreover, gamma-aminobutyric acid receptor type A (GABAA-R) represents a mechanistically crucial binding site in the LC for midazolam. Our findings will provide novel insights into the neural circuit mechanisms underlying the recovery of consciousness after midazolam administration and will help guide the timing of clinical dosing and propose effective intervention targets for timely recovery from midazolam-induced loss of consciousness.

Keywords: Midazolam; locus coeruleus (LC); norepinephrine (NE); ventrolateral preoptic nucleus (VLPO); gamma-aminobutyric acid receptor type A (GABAA-R); consciousness

Introduction

Midazolam has been extensively utilized in clinical practice for nearly half a century. This benzodiazepine exhibits rapid onset and a short duration of action, and causes relatively mild hemodynamic effects(Mandrioli et al., 2008; Reves et al., 1985). It induces anterograde amnesia, thereby averting intraoperative awareness and

mitigating the emergence of malignant memories in patients. The above characteristics of midazolam make it an indispensable drug for the treatment of psychiatric patients in the United States, China, Europe, and numerous other countries worldwide(Conway et al., 2016).

Psychiatric disorders globally constitute a significant source of severe, long-term disability and socioeconomic strain. Among these, Insomnia stands as a prevalent health issue in the general population and clinical settings(Perlis et al., 2022). The World Health Organization (WHO) reported that about 30% of the adult population worldwide suffer from insomnia, especially alongside other mental and physical health conditions(Sutton, 2021). Intractable insomnia frequently co-occurs with severe complications, including cognitive and immune decline, emotional disorders, and suicidal tendencies(Buysse, 2013; Gebara et al., 2018). Oral benzodiazepines, exemplified by midazolam, constitute the foundation of their therapy regimen(Riemann et al., 2015). Furthermore, agitation, a prevalent clinical issue in numerous psychiatric disorders, significantly copounds morbidity during hospitalization(Citrome, 2021). The extensively used medication for patients with acute agitation in the emergency department and intensive care unit is midazolam(Kim et al., 2021; Shafer, 1998). In conclusion, midazolam has emerged asone of the most commonly administered psychotropic drugs in clinical practice, effectively inducing a sedative response with diminished consciousness.

However, a critical challenge in the clinical application of midazolam pertains to its safety profile. Depending on the dose, it produces effects ranging from anxiolysis

61 to loss of consciousness, leading it to be versatile to have anxiolytic, sedative and
62 hypnotic effects(Kanto, 1985; Olkkola and Ahonen, 2008). Prolonged or excessive
63 midazolam administration frequently results in increased sedation accumulation and
64 depth, potentially causing delayed recovery, which in turn prolongs hospitalization
65 and precipitating diverse complications(Shehabi et al., 2012). Consequently, it is
66 imperative to investigate the mechanisms underlying midazolam-induced altered
67 consciousness and find promising targets to prevent its complications.

68 Midazolam has depressant effects on the central nervous system (CNS). It is
69 believed to act on the brainstem reticular formation and limbic system via
70 gamma-aminobutyric acid receptor type A (GABAA-R), reducing brain excitability
71 and inducing sedation. GABAA-R is the initiating molecular target of midazolam
72 action. However, the specific mechanism governing the regulatory systems
73 downstream of the GABAergic system in midazolam-induced alterations in
74 consciousness remains to be elucidated. Midazolam elicits and
75 electroencephalographic (EEG) pattern resembling normal non-rapid eye movement
76 (NREM) sleep, lacking a sustained long-range specific activation pattern compared to
77 wakefulness(Massimini et al., 2012). Therefore, we postulate that a
78 midazolam-induced loss of consciousness, at least partially, involves the activation of
79 an endogenous sleep-promoting pathway.

80 The LC serves as the primary site for norepinephrine (NE) synthesis and release
81 in the brain, exhibiting extensive projections to various other brain regions(Benarroch,
82 2018). The LC^{NE} neurons, which has been linked to multiple functions, including

83 sleep and arousal, stress-related behaviors, attention, and pain conduction, are
84 reportedly instrumental in sleep–arousal regulation(Poe et al., 2020; Suárez-Pereira et
85 al., 2022). Optogenetic activation of LC^{NE} neurons results in an instantaneous shift
86 from sleep to wakefulness(Carter et al., 2010). The ventrolateral preoptic nucleus
87 (VLPO) in the preoptic hypothalamus is recognized as a pivotal "sleep center" in
88 which sleep-activated neurons orchestrate the initiation and promotion of sleep, and
89 these neurons are subject to regulation by the LC^{NE} neurons(Chou et al., 2002; Sherin
90 et al., 1996, 1998). Recently, it has been reported that optogenetic activation of the
91 LC-VLPO NEergic neural circuit facilitates arousal from sleep, mediating its effect
92 through distinct adrenergic receptors, indicating the significance of this neural circuit
93 in controlling wakefulness(Liang et al., 2021). However, natural sleep is a
94 physiological state, whereas drug-induced loss of consciousness is a pathological state,
95 and the two are quite different from a pathophysiological perspective despite some
96 correlation. Furthermore, dexmedetomidine-induced sedation encompasses the
97 utilization of the endogenous sleep-promoting pathway mediated by the
98 LC-VLPO(Nelson et al., 2003). Therefore, these studies offer hints for additional
99 investigation into the role of LC-VLPO NEergic neural circuit in midazolam-induced
100 alterations in consciousness. This will facilitate a more targeted clarification of the
101 neural mechanisms underlying the sedative-hypnotic effects of midazolam, with
102 profound clinical implications.

103 In the current study, it was unveiled that midazolam initially functioned by acting
104 on GABAA-R in the LC. Crucially, we found that the LC-VLPO NEergic neural

circuit plays an important role in promoting recovery from midazolam and that this effect was primarily mediated by α1 adrenergic receptors (α1-R). We took a cascading approach from peripheral to central to validate our hypothesis. Initially, we used pharmacological methods to investigate the link between the NE system and awakening from midazolam administration. Subsequently, we adopted more precise and targeted approaches, such as optogenetics and chemogenetics to further substantiate our finding and successfully prove the involvement of the NEergic LC-VLPO neural circuit in facilitating the restoration of consciousness following midazolam administration. In addition, we employed both female and male mice in a series of chemogenetic activation experiments, suggesting that interventions that promoted rebooting from midazolam-induced unconsciousness in male mice were equally effective in female mice. In other words, our findings possess universal applicability and hold significant clinical application value. Based on the above experimental results, we further employed the knockdown technique to specifically manipulate GABAA-R on LC^{NE} neurons. We found that knockdown GABAA-R not only reduced recovery time from midazolam but also affected calcium signals in NEergic terminals at VLPO. More importantly, specifically block α1-R at VLPO reversed the effect of shortened recovery time produced by GABAA-R knockdown on LC^{NE} neurons.

These results will significantly enhance our understanding of the neural circuit mechanisms of midazolam-induced altered consciousness and provide a potential target for interventions aimed at addressing delayed recovery caused by midazolam.

127 ## Results

128 **The noradrenergic system contributes to recovering from midazolam**
129 **administration.**

130 Before starting the following experiments, we first determined the optimal
131 intraperitoneal (IP) dose of midazolam-induced sedation (loss of consciousness). We
132 chose the lowest effective dose that could induce LORR (loss of righting reflex)
133 successfully in all of the mice, i.e., 60 mg/kg, as the dose for the subsequent
134 experiments (Figure 1A-B).

135 To examine the role of the central noradrenergic system, we individually analyzed
136 the norepinephrine (NE) content in the prosencephalon and brainstem of mice (Figure
137 1C). Given that NE in the brain is mainly derived from the brainstem, the NE content
138 in the prosencephalon differed significantly from that in the brainstem under normal
139 conditions (P<0.0001, Figure 1D). However, we also found that compared with the
140 control group, the NE content in the brainstem was significantly reduced after
141 midazolam administration (P<0.05, Figure 1D).

142 Subsequently, we adopted a pharmacological method of peripheral intervention on
143 NE. We found that IP injection of atomoxetine (20 mg/kg), a central selective NE
144 reuptake inhibitor, increased the number of c-Fos (+)/TH (+) cells in the LC ($P < 0.01$,
145 Figure 1J, L) and shortened the recovery time from midazolam administration ($P <$
146 0.05, Figure 1F). In contrast, IP injection of
147 N-(2-chloroethyl)-N-ethyl-2-bromoben-zylamine hydrochloride (DSP-4) (50 mg/kg),
148 a highly selective NEergic neurotoxin, reduced the number of TH+ cells in the LC,

149 most significantly on day 10 after injection (P < 0.0001, Figure 1I, K) and prolonged
150 the recovery time from midazolam administration (*P* < 0.05, Figure 1G). Furthermore,
151 continuous IP injection of DSP-4 for 10 days significantly reversed the
152 recovery-promoting effects of atomoxetine (*P* < 0.01, Figure 1H). These findings
153 collectively indicate that the noradrenergic system contributes to the
154 midazolam-induced altered consciousness

155 **The activity of LC^{NE} neurons is significantly reduced after midazolam**
156 **administration**

157 Since LC is the largest nucleus in the brain that syntheses and releases NE, we
158 utilized fiber photometry to quantify the neuronal activity of LC^{NE} neurons at different
159 states after midazolam administration (Figure 2A-B). We injected
160 AAV2/9-DβH-GCaMP6m-WPRE-hGH pA with a specific promoter into the bilateral
161 LC of C57BL/6J mice to express the GCaMP6m calcium indicator specifically in
162 NEergic neurons and examined changes in GCaMP6m fluorescence signal through an
163 optical fiber located in the LC (Figure 2C-D). During the LORR to RORR (recovery
164 of righting reflex) phase, we found that the ΔF/F peak of calcium signaling in LC^{NE}
165 neurons was significantly reduced compared with other phases, and then increased
166 after RORR (*P* < 0.05, *P* < 0.01, Figure 2E-H).

167 To further evaluate the changes in neuronal activity in the LC following midazolam
168 administration, we performed immunofluorescence staining for c-Fos and TH.
169 Fluorescence images revealed a reduction in the number of c-Fos-positive cells
170 co-labeled with TH in the midazolam administration group compared to the control

171 group (P < 0.01, Figure 2I-K). These results indicated that LC^{NE} neurons were
172 significantly inhibited after midazolam administration.

173 **LC^{NE} neurons contribute to regulating recovery from midazolam**

174 To delve deeper into of LC^{NE} neurons in recovery after midazolam administration,
175 we artificially intervened in LC^{NE} neurons. We microinjected DSP-4 into LC to
176 specifically degrade LC^{NE} neurons and found a significant decrease in the number of
177 TH+ neurons in the LC of mice 10 days after the DSP-4 microinjection ($P < 0.0001$,
178 Figure 2P-Q). Furthermore, microinjecting DSP-4 into LC not only significantly
179 extended the recovery time from midazolam-induced loss of consciousness but also
180 attenuated the recovery-promoting effect of intraperitoneally administered
181 atomoxetine (P < 0.05, Figure 2N-O). These suggest that intranuclear administration
182 of DSP-4 to specifically ablate LC^{NE} neurons postpone recovery from midazolam
183 administration.

184 Then, optogenetic manipulation was used to further examine the role of LC^{NE}
185 neurons (Figure 3A-B). For this purpose, we combined a Cre-dependent AAV
186 expressing channelrhodopsin-2 (ChR2) fused with enhanced yellow fluorescent
187 protein (AAV-DIO-ChR2–eYFP) with Cre-AAV expressing the TH promoter
188 (TH-Cre-AAV) to restrict the expression of ChR2 to LC TH+ neurons and an optrode
189 was implanted at the injection site (Figure 3C-D). Our results showed
190 photostimulation (20 min/4mW) of LC^{NE} neurons significantly shortened the recovery
191 time and produced a pro-recovery effect from midazolam regardless of whether it was
192 left, right, or bilateral LC optogenetic activation ($P < 0.05$, Figure 3E-G). Additionally,

193 fluorescence images revealed a significant increase in the number of c-Fos (+)/TH (+)
194 cells after photostimulation of LC^{NE} neurons ($P < 0.0001$, Figure 3H-J).

195 Next, we tested whether the chemogenetic activation of LC^{NE} neurons promotes
196 recovery (Figure 3K). In order to reveal whether there was sex discrepancy in
197 chemogenetic activation of LC^{NE} neurons, we used both male and female mice, and
198 Cre-dependent excitatory DREADD was co-infused with TH-Cre-AAV to restrict the
199 expression of hM3Dq to LC TH+ neurons (Figure 3L). We determined the
200 transfection efficiency of the chemogenetic virus in LC^{NE} neurons (Figure 3M-O).
201 Similar results were obtained in the chemogenetic experiment. We found that in both
202 male and female mice, IP injection of 0.2 mg/kg CNO could shorten the recovery time
203 and produce a pro-recovery effect from midazolam regardless of whether it was left,
204 right, or bilateral LC chemogenetic activation ($P < 0.05$, Figure 3P-S). Additionally,
205 c-Fos (+)/TH (+) cells were significantly increased after photostimulation of LC^{NE}
206 neurons ($P < 0.0001$, Figure 3T-V). Thus far, we have proven that there was no sex
207 discrepancy in chemogenetic activation of LC^{NE} neurons, and LC^{NE} neurons
208 contribute to the recovery from midazolam.

209 **Activation of the LC-VLPO NEergic neural circuit promotes recovery from**
210 **midazolam**

211 The LC sends projections to several brain regions, including the VLPO, which is
212 a crucial area in regulating sleep and arousal states. Therefore, we hypothesized that
213 LC and VLPO interact to mediate midazolam-induced alterations in consciousness. To
214 confirm the existence of the LC–VLPO projection, we microinjected the mix of

mTH-Cre-AAV and AAV-EF1a-DIO-hChR2(H134R)-eYFP viruses into the LC and microinjected rAAV2/9-DβH-GCaMP6m-WPRE-hGH pA into the VLPO. Two weeks later, optical fibers were implanted into the VLPO to record neuronal firing (Figure 4A-B). We observed local NEergic terminals within the VLPO (Figure 4D, K). Also, we found that optogenetic or chemogenetic activation of LC^{NE} neurons resulted in an enhanced ΔF/F peak in the VLPO ($P < 0.05$, $P < 0.01$, Figure 4O-X), i.e., increased VLPO activity, as well as facilitated recovery from midazolam ($P < 0.05$, Figure 4G, M-N). Moreover, we found that there was no sex discrepancy in chemogenetic studies.

To further identify whether the LC-VLPO NEergic circuit mediates promoting recovery, we used optogenetics to activate LC^{NE} terminals in the VLPO. We injected the mixture of DBH-Cre-AAV and AAV-EF1a-DIO-hChR2(H134R)-eYFP viruses into bilateral LC and AAV-EF1a-DIO-hChR2(H134R)-eYFP virus into bilateral VLPO, then implanted optical fibers above the VLPO (Figure 5A-B). Immunofluorescence results showed expression of hChR2 in the VLPO (Figure 5F). It confirms the structural association between the LC and the VLPO. In addition, when the NEergic terminals of the LC-VLPO pathway were photostimulated with blue light, we observed a shorter recovery time in the VLPO photostimulation group compared to the non-photostimulation group ($P < 0.01$, Figure 5G). Thus, optogenetic activation of VLPO-projecting LC^{NE} neurons promotes recovery from midazolam. Next, we tested whether the chemogenetic activation of LC^{NE} terminals in the VLPO promotes recovery (Figure 5H, I). We injected the mixture of DBH-Cre-AAV and

237 AAV-Ef1a-DIO-hM3Dq-mCherry viruses into bilateral LC and
238 AAV-Ef1a-DIO-hM3Dq-mCherry virus into bilateral VLPO, then implanted cannula
239 above the VLPO to inject CNO (20ug/ml,400nl). In order to reveal whether there was
240 sex discrepancy in chemogenetic activation of LC^{NE} neurons, we used both male and
241 female mice. (Figure 5J-N). Similar results were obtained in the chemogenetic
242 experiment. We found that in both male and female mice, intra-VLPO microinjection
243 of CNO could produce a pro-recovery effect from midazolam ($P < 0.05$, Figure 5N).
244 Thus far, our results show the contribution of the LC-VLPO NEergic neural circuit in
245 regulating midazolam-induced altered consciousness.

246 **The promotion of recovery from midazolam is primarily mediated by the α1**
247 **adrenergic receptor**

248 To identify the role of different types of noradrenergic receptors in the brain, we
249 used a pharmacological approach. By intracerebroventricular (ICV) injection of
250 different doses of α1-R, α2-R, and β-R agonists and antagonists (Figure 6A), we
251 found that the α1 receptor agonist phenylephrine (20mg/mL) significantly shortened
252 recovery time from midazolam ($P < 0.05$, Figure 6C). Conversely, the α1 receptor
253 antagonist prazosin (1.5mg/mL), the α2 receptor agonist clonidine (1.5mg/mL), and
254 the β receptor antagonist propranolol (5mg/mL) caused the opposite effects ($P < 0.05$,
255 Figure 6D, E, H). However, the α2 receptor antagonist yohimbine and the β agonist
256 isoprenaline did not affect the recovery time ($P > 0.05$, Figure 6F-G), and
257 phenylephrine significantly reversed the effect of propranolol in prolonging recovery
258 time from midazolam ($P < 0.01$, Figure 6I). These results indicate that the recovery

259 from midazolam is mediated predominantly by α1-R.

260 **The pro-recovery effect of activating LC^{NE} neurons can be reversed by ICV**
261 **injection or intra-VLPO microinjection of α1-R antagonist**

262 To further determine the link between the LC and VLPO, we assessed the effect
263 of photostimulation and pharmacology (Figure 6J). A mixture of the Cre-dependent
264 AAV vector Ef1a-DIO-hChR2(H134R)-eYFP and mTH-Cre-AAV was injected
265 bilaterally into the LC, and optical fibers were implanted (Figure 6K). 2 weeks later,
266 drug-delivery cannulas were implanted into the ICV or VLPO (Figure 6M, O). Then,
267 we injected prazosin through cannulas within the ICV or VLPO to block α1-R and
268 activate LC by photostimulation to further observe the effects of both on midazolam
269 recovery time. The results showed that photostimulation of LC^{NE} neurons could
270 reduce the recovery time ($P < 0.05$), whereas prazosin could prolong the recovery
271 time ($P < 0.05$), and that prazosin reversed the effects produced by LC activation ($P <$
272 0.01, $P < 0.001$, Figure 6N, P). Meanwhile, to further assess the effect of the above
273 maneuvers on the depth of sedation, we performed EEG recordings. We found that
274 cortical EEG activity was significantly reduced after LORR in all groups and
275 remained at a low level during the LORR to RORR, while optogenetic activation
276 of LC resulted in some high-amplitude EEG activity (Figure 7A-C), implying that
277 LC^{NE} activation may affect the depth of sedation.

278 A similar experiment was conducted utilizing the chemogenetic approach (Figure
279 6Q). The mixture of mTH-Cre-AAV and AAV-Ef1a-DIO-hM3Dq-mCherry viruses
280 was injected into bilateral LC (Figure 6R); 2 weeks later, we determined the

281 transfection efficiency of the chemogenetic virus in LC^{NE} neurons in both male and
282 female mice (Figure 6S, X). For male mice, bilateral drug-delivery cannulas were
283 implanted into the ICV or VLPO (Figure 6T, V); For female mice, bilateral
284 drug-delivery cannulas were implanted into the VLPO (Figure 6Y). α1-R antagonist
285 was microinjected through the cannulas and behavioral tests were conducted as well
286 as EEG recordings. Consistent with the above results, in male mice, both ICV and
287 intra-VLPO injections of prazosin prolonged the recovery time ($P < 0.01$, $P < 0.05$),
288 and reversed the pro-recovery effect produced by chemogenetic activation of LC^{NE}
289 neurons ($P < 0.01$, Figure 6U, W). Also, in female mice, intra-VLPO injections of
290 prazosin prolonged the recovery time ($P < 0.05$), and reversed the pro-recovery effect
291 produced by chemogenetic activation of LC^{NE} neurons ($P < 0.001$, Figure 6Z). In
292 addition, chemogenetic activation of LC leads to some high-amplitude EEG activity
293 (data from male mice, Figure 7D-F).

294 In summary, the recovery-promoting effects of all the aforementioned
295 interventions, which activate LC^{NE} neurons can be reversed by prazosin. We further
296 established the existence of a functional connection between LC^{NE} neurons and VLPO
297 that co-regulates recovery after midazolam. Notably, α1-R on the VLPO is the
298 downstream target involved in the mechanism of recovery from midazolam.

299 **GABAA-R is an important mechanical binding site for midazolam in the LC**

300 Midazolam is a short-acting central benzodiazepine receptor inhibitor that acts
301 primarily on GABAA-R, thus increasing GABAergic neurotransmission and
302 depressing the CNS. Hence, we further explored whether LC^{NE} neurons exert their

303 effects through GABAA-R after midazolam administration. We microinjected
304 GCaMP6m into the LC in mice and implanted an optical fiber to observe changes in
305 LC calcium signaling after the injection of gabazine, a GABAA receptor antagonist,
306 into the lateral ventricle or LC (Figure 8A). We found that compared with the vehicle,
307 ICV injection and intra-LC microinjection of 4μg/mL gabazine could reduce the
308 recovery time ($P < 0.05$, Figure 8C, E). In addition, gabazine could increase the ΔF/F
309 peak of calcium signaling in LC^{NE} neurons before LORR and during the RORR to
310 Recovery phase ($P < 0.05$, Figure 8H-K). These data indicate that GABAA-R in LC
311 may be the initiating binding site of midazolam to produce altered consciousness.

312 We have already demonstrated that midazolam affects LC^{NE} neuronal activity via
313 GABAA-R in the LC, which then exerts its effects via downstream α1-R. First,
314 drug-delivery cannulas were implanted into the LC and VLPO, respectively. One
315 week later gabazine was injected into the LC to block GABAA-R, while prazosin was
316 injected into the VLPO to antagonize α1-R (Figure 8L-M). We found that
317 microinjection of gabazine into the LC could reduce the recovery time ($P < 0.05$),
318 whereas microinjection of prazosin into the VLPO could increase the recovery time (P
319 < 0.05, Figure 8O). In addition, we found that microinjection of prazosin into VLPO
320 prolonged the recovery time and significantly reversed the blockade of LC
321 GABAA-R-induced pro-recovery effect ($P < 0.05$, $P < 0.001$, Figure 8O).

322 To investigate the role of GABAA-R on LC^{NE} neurons in the modulation of
323 recovery from midazolam, we performed a loss-of-function study using shRNA to
324 knockdown GABAA-R in the bilateral LC^{NE} neurons. As assessed by

325 immunofluorescence staining analysis, the expression of GABAA-R on LC^{NE} neurons
326 was significantly reduced compared to the sham group ($P<0.0001$, Figure 9A-F). We
327 found that knockdown of GABAA-R prolonged the recovery time from midazolam,
328 while did not affect the dose of midazolam-induced LORR ($P<0.01$, Figure 9G-I).

329 **GABA-ergic and NE-ergic systems interact with each other, co-regulate the**
330 **recovery from midazolam**

331 In previous experiments, we preliminarily proved that GABA-ergic and NE-ergic
332 systems co-regulate recovery from midazolam by the pharmacological method. Then,
333 we combined the gene knockdown technique with fiber photometry to delve deeper
334 (Figure 9J-Q). We found that the ΔF/F peak of calcium signaling in the VLPO
335 NE-ergic terminals in the shRNA group was significantly reduced compared with the
336 sham group ($P<0.05$, Figure 9R-T).

337 More importantly, we knocked down GABAA-R on LC^{NE} neurons, resulting in
338 fewer targets for midazolam and weakened function of the GABA-ergic system, and
339 similar to previous results, recovery time from midazolam was reduced. Meanwhile,
340 microinjecting NE α1-R antagonist in the VLPO, we found that the reduction of
341 recovery time caused by the knockdown of GABAA-R was reversed ($P<0.05$, Figure
342 9Z), suggesting that the NE-ergic system is indeed involved in recovering from
343 midazolam with NE α1-R on VLPO neurons is an important functional site in the
344 LC-VLPO neural circuit.

345 Discussion

346 Midazolam holds significant potential in the treatment of psychiatric disorders as

347 sedative-hypnotics. Although the number of clinical studies addressing the effects of
348 midazolam on consciousness as well as behavior is gradually increasing, the specific
349 neural mechanisms by which it alters consciousness remain unclear. To fill this gap,
350 we opted to investigate midazolam, a clinical drug, to study in mice to find a
351 promising target for the development of an effective strategy to provide targeted
352 therapies for the reversal of midazolam-induced delayed recovery.

353 In the current study, we employed a cascade approach, initially utilizing
354 pharmacology and ELISA to validate that the central NE system plays an important
355 role in recovery from midazolam sedation. We found that midazolam administration
356 significantly reduced NE content in the brainstem, whereas IP injection of
357 atomoxetine, an NE reuptake inhibitor, could shorten recovery time from midazolam.
358 Conversely, peripheral injection of DSP-4 reverses the pro-recovery effect of
359 atomoxetine. Second, based on calcium signaling, we found a decrease in LC^{NE}
360 neuronal activity after midazolam administration. Concordantly, optogenetic and
361 chemogenetic activation of LC^{NE} neurons could facilitate recovery from midazolam,
362 whereas elective ablation of LC^{NE} neurons by intra-LC microinjection of DSP-4
363 attenuates recovery. Third, we turned our attention to the downstream pathway of the
364 LC. We found that optogenetic and chemogenetic activation of LC^{NE} neurons could
365 influence the activity of VLPO, and ChR2 can be transmitted from the LC to the
366 VLPO across synapses, suggesting that the LC can project to the VLPO. Next, ICV
367 injection of different adrenergic receptor agonists or antagonists suggested the main
368 involvement of α1-R in the regulative effect of recovery from midazolam. Also, we

369 microinjected α1-R antagonist into VLPO, and we found that the pro-arousal effect
370 induced by activation of LC^{NE} neurons was reversed, suggesting that α1-R in the
371 VLPO is more responsive to regulate recovery from midazolam. Then, ICV injection
372 of the GABAA-R antagonist gabazine or microinjection of gabazine into the LC
373 shortened the recovery time from midazolam, and we found that antagonizing
374 GABAA-R could inhibit the activity of LC, suggesting that GABAA-R in the LC may
375 be an initiating target for the action of midazolam. Finally, by using pharmacological
376 method and gene knockdown technique we found that GABA-ergic and NE-ergic
377 systems co-regulated recovery from midazolam, and GABAA-R on LC^{NE} neurons and
378 NE α1-R on VLPO were the key points. More importantly, in this study, both male
379 and female mice were used in all chemogenetic activation experiments, and we found
380 that sex discrepancies did not affect the results of the experiment, which signified that
381 the intervention that promoted rebooting from midazolam-induced unconsciousness
382 was equally effective in both male and female mice. Our findings have a universal
383 applicability as well as great clinical translational significance. For the DBH promotor
384 applied in the optogenetic and chemogenetic studies, as supported by the literature,
385 DBH (Dopamine-beta-hydroxylase), located in the inner membrane of noradrenergic
386 and adrenergic neurons, is an enzyme that catalyzes the conversion of dopamine to
387 norepinephrine, and therefore plays an important role in noradrenergic
388 neurotransmission. DBH is a marker of noradrenergic neurons. Zhou et al. (2020)
389 clarified the probe specifically labeled noradrenergic neurons by immunolabeling for
390 DBH. Recently, DBH promoter have been used in several studies (e.g., Han et al.,

391 2024; Lian et al., 2023). The DBH-Cre mice are widely used to specifically labeled
392 noradrenergic neurons (e.g., Li et al., 2023; Breton-Provencher et al., 2022; Liu et al.,
393 2024). It is difficult to distinguish the role of NE or DA neurons when using the TH
394 promoter in VLPO. Therefore, we used DBH promoter with more specific labeling.
395 LC is the main noradrenergic nucleus of the central nervous system. In our study, we
396 injected rAAV-DBH-GCaMP6m-WPRE (Figure 2 and 8) and
397 rAAV-DBH-EGFP-S'miR-30a-shRNA GABAA receptor)-3'-miR30a-WPRES (Figure
398 9) into the LC. The results showed that DBH promoter could specifically label
399 noradrenergic neurons in the LC, while non-specific markers outside the LC were
400 almost absent.

401 Altered states of consciousness attributed to the action of sedative drugs on
402 molecular targets in the CNS have been the focus of research over the past decades.
403 GABAA-R is a well-recognized target of different sedative agents. GABAA-R is a
404 ligand-gated Cl- channel that mediates the majority of the fast inhibitory
405 neurotransmission in the CNS and has a crucial role in regulating brain excitability.
406 The GABAA-R family comprises 19 subunit genes, including α1–6, β1–3, γ1–3, δ, ε,
407 θ, π, and ρ1–3, which assemble to form a pentameric structure(Ghit et al., 2021). The
408 GABAA-R has a GABA-binding receptor site and some regulatory sites for binding
409 of various substances, and the best characterized regulatory site is the benzodiazepine
410 (BZ) one(Sigel and Ernst, 2018). Midazolam is a prevalent psychotropic substance
411 that acts as a positive allosteric modulator of this receptor(Olsen, 2018). The drug
412 binds highly specifically to the BZ-binding site on the GABAA-R complex,

413 modulating the affinity of GABA and GABA-binding receptor sites and reducing the
414 excitability of the CNS, thus inducing sedation, hypnosis, and unconsciousness.
415 Receptors containing the α1, 2, 3, 5 and γ2 subunit interface form the BZ-binding site
416 of GABAA-R, suggesting the significance of these subunits in midazolam-mediated
417 effects(Maramai et al., 2020). Notably, β3-knockout mice exhibit a shorter duration
418 of loss of righting reflex (LORR) in response to midazolam, suggesting a role of β
419 3-containing GABAA-R in mediating midazolam-induced unconsciousness (Quinlan
420 et al., 1998). According to our findings, midazolam modulates downstream neural
421 pathways by initially acting on GABAA-R in the LC. It is future studies of membrane
422 proteins and ion channels in LC or non-LC NEergic neurons that we call for to fully
423 understand the molecular and neural circuit targets of sedative-hypnotics.

424 Midazolam elicits a de-consciousness state resembling natural sleep, likely
425 involving endogenous sleep-arousal neural nuclei and circuits to induce hypnosis and
426 loss of consciousness. In conjunction with past studies, midazolam and other sedative
427 drugs act primarily by enhancing GABAergic inhibitory neurotransmission, implying
428 a sleep-like facilitating effect of the GABAergic system. However, the mechanism of
429 neural circuits downstream of GABA that regulate changes in consciousness remain
430 elusive.

431 Arousal in the brain depends on many areas that can simultaneously receive
432 diverse signals, with the ascending reticular activating system (ARAS) overseeing
433 arousal and wakefulness maintenance(Lee and Dan, 2012). LC^{NE} neurons, which are
434 an important component of the ARAS, reportedly play a key role in the maintenance

435 of arousal and alertness(Berridge et al., 2012). Specifically, we posit that LC^{NE}
436 neurons and their associated circuits are involved in modulating recovery from
437 midazolam. In this study, LC^{NE} neurons were activated by photostimulation and
438 chemogenetics to rapidly induce the transition from unconsciousness to awakening.
439 As a pivotal arousal center, the LC receives arousal-related inputs and extensively
440 innervates the cerebral cortex and forebrain structures with NEergic projections(Hayat
441 et al., 2020). We initially pharmacologically validated the role of the central NEergic
442 system in modulating midazolam recovery. Subsequently since the LC is the
443 predominant nucleus in the brain for the release of NE, we further demonstrated the
444 role of LC^{NE} neurons in midazolam recovery through selective activation and
445 degradation of them. Here, our study elucidates the critical role of NEergic neurons in
446 the LC in midazolam recovery by pharmacology, optogenetics and chemogenetics.

447 Given that the VLPO lies downstream of the LC and plays a crucial role in
448 sleep-related information integration, we spotlighted the LC-VLPO neural circuit. The
449 VLPO harbors diverse neuronal populations, including GABAergic and galaninergic
450 neurons, which are recognized as sleep-active neurons(Arrigoni and Fuller, 2022).
451 Intriguingly, there is another cluster of glutamatergic neurons in the VLPO that
452 promote arousal(Chung et al., 2017; Vanini et al., 2020). A recent report showed that
453 LC^{NE} neurons synergistically facilitate arousal from sleep by simultaneously
454 activating wake-active neurons and inhibiting sleep-active neurons in the VLPO. This
455 regulation of the two types of neurons in the VLPO is mediated by distinct adrenergic
456 receptors(Liang et al., 2021). However, our study differs significantly. First, we

457 demonstrate that LC may play an irreplaceable role in midazolam-induced loss of
458 consciousness because atomoxetine is a reuptake inhibitor of widespread NE in the
459 brain, but our selective disruption of LC rendered its effect lost. Second, our study
460 pinpoints GABAA-R in the LC as a potential key target for midazolam's effects. Third,
461 we identified this α1 receptor as a necessary target through pharmacology and further
462 validated it with more specific means. Finally, we found that intra-VLPO
463 microinjection of the α1 receptor antagonist prazosin significantly reversed the
464 pro-recovery effect of intra-LC microinjection of GABAA receptor antagonist or
465 activation of LC^{NE} neurons. Crucially, atomoxetine, a psychotropic drug for treating
466 attention-deficit hyperactivity disorder (ADHD), is a promising candidate for
467 translational research to prevent delayed recovery from midazolam abuse in patients
468 with ADHD. Essentially, targeting the central α1-R, particularly in VLPO wake-active
469 neurons, may yield rational therapeutic strategies to prevent delayed recovery.
470 Notably, the VLPO in turn sends GABAergic inhibitory projections to various
471 wake-promoting nuclei throughout the neuroaxis, including the LC(Saper et al., 2005).
472 Studies indicate that the activated VLPO releases GABA to the LC, thus inducing
473 NREM sleep, while NE released from the activated LC inhibits VLPO sleep-active
474 neuron activity and promotes wakefulness(Brown et al., 2012; Van Egroo et al., 2022).
475 As such, a deeper exploration of the interactions between diverse VLPO neuronal
476 populations and their specific connections with the LC is warranted in our study.

477 The translational implications of a study are indeed a crucial measure of its
478 significance. Our current study has the potential to translate into guidance for the

479 clinical use of midazolam and allow for reducing unwanted drug side effects. On the
480 one hand, we have selected the clinical drug midazolam for animal experiments,
481 which will help us to develop useful drugs to treat midazolam-induced serious
482 complications (e.g., delayed recovery, ventilator-associated pneumonia, and coma) in
483 the future, thus further advancing clinical trials. It provides some hints for managing
484 agitated patients with neuropsychiatric disorders. On the other hand, in addition to
485 intravenous or intramuscular administration, midazolam can also be taken orally to
486 treat insomnia, ameliorate anxiety, and treat seizures and status epilepticus(Conway et
487 al., 2016; Nordt and Clark, 1997; Smith and Brown, 2017). Oral midazolam affects
488 consciousness to a greater or lesser extent, and some suicidal patients have even
489 suffered immediate death from massive doses of midazolam. Our study thus offers
490 valuable insights for medication guidance in such cases.

491 In summary, our study demonstrates that, in mice, the LC-VLPO NEergic neural
492 circuit contributes to the rapid modulation of altered consciousness induced by
493 midazolam, which is essential to ameliorate the complications of its abuse. It will
494 pinpoint the relevant regions involved in response to midazolam and provide a
495 perspective to help elucidate the dynamic changes of neural circuits in the brain
496 during altered consciousness. It suggests a promising new avenue of investigation for
497 the targets of timely recovery from midazolam-induced loss of consciousness, thereby
498 minimizing the risk of delayed recovery and associated complications.

499 **Limitations**

500 This study shows that the LC-VLPO NEergic neural circuit plays an important

role in modulating midazolam recovery. However, the specificity of LC NE downstream neurons in the VLPO is not explained in this paper, which is our next research direction, VLPO neurons and their downstream regulatory mechanisms may be involved in other nervous systems except the NE nervous system, and the deeper and more complex mechanisms need to be further investigated. In addition, given the pharmacological actions of midazolam, other areas may also be involved. Current studies suggest that the neural network involved in the recovery of consciousness consists of the prefrontal cortex, basal forebrain, brain stem, hypothalamus and thalamus (Nguyen and Postnova, 2021). The role of these regions in midazolam recovery remains to be further investigated. Therefore, we will apply more specific experimental methods to determine the importance of LC-VLPO NEergic neural circuit and related NE receptors in the midazolam recovery, and conduct further studies on other relevant brain neural regions, hoping to more fully elucidate the mechanism of midazolam recovery in the future.

Materials and methods

Ethics

This study was approved by and all experimental procedures were performed in compliance with the Experimental Animal Ethics Committee of Zhejiang University.

Animals

The experimental animals in this study were male and female wild-type C57BL/6J mice purchased from the Animal Experiment Center of Zhejiang University. All mice were housed and bred in the SPF-Class House in a standard condition (indoor

523 temperature 25 ℃, ambient humidity 65%, 12-h/12-h light/dark cycle) with rodent
524 food and water available *ad libitum*. All mice were aged 8 weeks and weighed 22–25
525 g at the start of the experiments. All experiments were mainly performed between
526 9:00 and 16:00.

527 **Establishment of a mice model of midazolam administration**

528 We randomly divided healthy C57BL/6J mice into four groups (n = 8). These mice
529 were used to determine the intraperitoneal dose of midazolam that would achieve the
530 optimal depth without inhibiting respiration before starting the formal experiment.
531 Finally, we identified the lowest effective dose that was 100% successful in inducing
532 loss of consciousness in mice, i.e., 60 mg/kg midazolam (H-19990027, Jiangsu Nhwa
533 Pharmaceutical Co., Ltd.), as the optimal dosage for intraperitoneal administration in
534 mice, and used this dose in subsequent experiments.

535 **Evaluation of recovery time**

536 Before the experiment, the bottom of the open box with no lid and air circulation was
537 covered with cotton pads, and an electric blanket was placed on the lower side of the
538 open box, and the temperature in the open box was preheated for 10 min before the
539 experiment to keep the temperature in the open box suitable and constant during the
540 experiment. Eight-week-old C57BL/6J mice were placed in the open box for 30 min,
541 and then placed in the open box again after intraperitoneal injection of the appropriate
542 dose of midazolam (60 mg/kg) to start the timer. At the same time, the open box was
543 gently rotated every 15 s. When the mice were rotated to the dorsal recumbent
544 position and could not be voluntarily turned over for more than 1 min, it was the loss

545 of righting reflex (LORR), i.e., loss of consciousness from midazolam. Subsequently,
546 the mice were placed in the dorsal recumbent position for continuous observation, and
547 when the mice could autonomously return to the normal position from the dorsal
548 recumbent position, they were considered as recovery of righting reflex (RORR). The
549 time from the onset of LORR to RORR was recorded as the Recovery Time of
550 midazolam.

551 **Enzyme-linked immunosorbent assay (ELISA)**

552 The tyrosine hydroxylase (TH) content and specific enzyme activity were measured in
553 two groups of C57BL/6J mice (n = 6 per group), one group was given 60mg/kg
554 midazolam intraperitoneally and the other group was not. The whole brain was
555 removed and sectioned, and then prosencephalon and brainstem tissue samples were
556 collected separately, and TH levels in these tissues were measured using an
557 enzyme-linked immunosorbent assay (ELISA) kit according to the manufacturer's
558 instructions (YS-M195, YS-M195-1, ELISA Kit, Yan Sheng Biological Technology
559 Co., Ltd., Shanghai, China). The optical density (OD) was measured at 450 nm and
560 630 nm using an ELISA microplate reader (SynergyMax M5, iD5, Molecular Devices,
561 San Jose, CA, USA).

562 **Stereotaxic surgery and virus microinjection surgery**

563 Eight-week-old C57BL/6J mice were weighed and injected intraperitoneally with 30
564 mg/kg of pentobarbital, and placed in the rearing cage for about 5~10 min. After
565 complete anesthesia, the mice were fixed on a stereotactic apparatus (68018, RWD
566 Life Sciences, Shenzhen, China), and the head hairs of the mice were shaved off with

567 a razor. A heating pad was used to maintain the body temperature of mice at 37°C
568 during the procedure, and an ophthalmic ointment was applied to their eyes to avoid
569 dryness. To expose the skull, the scalp was sterilized and a longitudinal incision was
570 made. The periosteum was then removed with 3% hydrogen peroxide and the residue
571 was rinsed with saline. After drilling holes in the skull, the virus was injected into the
572 target site at a flow rate of 40nL/min via an ultramicro pump (160494 F10E, WPI).
573 We left the needle at the target site for 10 min after injection to allow for diffusion of
574 the virus. To target the LC, the coordinates were AP: −5.41 mm; ML: ±0.9 mm; DV:
575 −3.8 mm. To target the VLPO, the coordinates were AP: −0.01 mm; ML: ±0.65 mm;
576 DV: −5.7 mm. To target the lateral ventricular, the coordinates were AP: −0.47 mm,
577 ML: −1.00 mm, DV: −2.40 mm. According to the experimental needs, optical fibers
578 or catheters were subsequently implanted in the corresponding location and secured
579 with dental cement. After that, the incision was sutured and the mice were placed on a
580 heating blanket to be transferred to a cage when the mice were awake.

581 **Optogenetics**

582 Three weeks before the experiment began, the LC or VLPO was microinjected with
583 an optogenetic virus of 100 nL of a 1:3 volume mixture of mTH-Cre-AAV/DBH-Cre
584 and AAV-EF1a-DIO-hChR2(H134R)-eYFP (viral titer: 5.00×10^{12}vg/mL, Brain VTA
585 Technology Co., Ltd., Wuhan, China). One week before the experiment began, the LC
586 or VLPO was implanted with optical fibers (FOC-W-1.25-200-0.37-3.0, Inper,
587 Hangzhou, China). TH-hChR2 expression in the LC and VLPO was determined by
588 immunohistochemistry after the completion of optogenetic experiments. The mice

589 were intraperitoneally injected with midazolam, and 20 min later, they were given 465
590 nm blue light to activate neurons in the LC or VLPO. In this study, we used different
591 parameters for optogenetic activation: 20 min/2mW; 20 min/4mW; 10 min/4mW; and
592 20 min/4mW. We finally identified 20 min/4mW as the optimal optogenetic activation
593 parameter and used it in the subsequent experiments.

594 **Chemogenetics**

595 Three weeks before starting the experiment, chemogenetic viruses of 100 nL of a 1:3
596 volume mixture of mTH-Cre-AAV/DBH-Cre and pAAV-EF1a-DIO-hM3D-mCherry
597 (viral titer: 5.00×10^{12}vg/mL, Brain VTA Technology Co., Ltd., Wuhan, China) were
598 microinjected into the LC or VLPO, and TH-hM3Dq expression in the LC and VLPO
599 was determined by immunohistochemistry after the completion of chemogenetic
600 experiments. Clozapine-N-oxide (CNO) (HY-17366, MedChemExpress) was
601 dissolved in saline, and the mice were intraperitoneally injected with CNO 20 min
602 after intraperitoneally injected with midazolam to activate neurons using the
603 chemogenetics approach. In this study, we tested two concentrations of CNO: 0.1
604 mg/kg and 0.2 mg/kg. We concluded that 0.2 mg/kg was the optimal concentration
605 and used this concentration for the subsequent intraperitoneal administration.

606 **Fiber photometry**

607 We microinjected 100nL of rAAV-DβH-GCaMP6m-WPRE-hGH pA (viral titer:
608 2.00×10^{12}vg/mL, Brain VTA Technology Co., Ltd., Wuhan, China) into the LC or
609 VLPO. Two weeks later, an optical fiber (FOC-W-1.25-200-0.37-3.0, Inper,
610 Hangzhou, China) was implanted in the same area located 0.05 mm above the virus

injection point (AP: −5.41 mm; ML: ±0.9 mm; DV: −3.75 mm/AP: −0.01 mm; ML: ±0.65 mm; DV: −5.65 mm) and fixed in place with dental cement. Three weeks after viral expression and one week after fiber optic placement, the calcium activity of the target neurons was monitored. Fluorescence emissions were recorded using a fiber photometry system (Inper, Hangzhou, China, C11946) using a 488-nm diode laser, and the mice were placed in a dark box to avoid the influence of natural light source on calcium signal recording, and accessed to the computer recording software to record calcium signals. After the recording was completed, the results recorded by the optical fiber were read into the calcium signaling data analysis software. The calcium signalings were recorded 30 min before LORR when the mice were awake. Then, midazolam was injected intraperitoneally. After the RORR, the experiment was terminated after 10 min of optical fiber recording. In Fig. 2, the time points for awake, midazolam injection, LORR and RORR in mice were respectively selected as time=0, while in Fig. 4, RORR in mice was selected as time=0. The selected traces lasting for 20s was based on the length of a complete Ca2+ signal. And the calcium signal intensity was calculated as the value of $\Delta F/F=(F-F0)/F0$.

GABAA-R Knockdown

We microinjected 80nL of rAAV-DBH-EGFP-S'miR-30a-shRNA (GABAA receptor)-3’-miR30a-WPRES (viral titer: 5E+12 vg/mL, Brain VTA Technology Co., Ltd., Wuhan, China) into the LC. Four weeks later, these mice were sacrificed and perfused for counting the GABAA-R (+) and tyrosine hydroxylase-positive (TH+) cells to evaluate the effect of GABAA-R knockdown.

633 **Pharmacological experiments**

634 **Effects of intraperitoneal injection of atomoxetine and DSP-4 and their**
635 **interaction on the recovery time of midazolam**

636 Atomoxetine (Ca #Y0001586, Sigma-Aldrich) which selectively inhibits presynaptic
637 uptake of norepinephrine (NE) and enhances norepinephrine function, was dissolved
638 in saline. One hour before intraperitoneal injection with midazolam, C57BL/6J mice
639 received intraperitoneal (IP) injection of atomoxetine (10 mg/kg or 20 mg/kg) or
640 saline (vehicle). To evaluate the impact of peripheral injection of atomoxetine on the
641 recovery time of midazolam, three trials were done for each group of mice (vehicle,
642 10 mg/kg, and 20 mg/kg), and the recovery time was recorded.

643 To further verify the effect of norepinephrine on the recovery time of midazolam,
644 we used DSP-4 (C8417, Sigma-Aldrich), a selective neurotoxin that targets the LC
645 norepinephrine system in the rodent brain and is used to disrupt nerve terminals and
646 attenuate NE and NE transporter function in the LC-innervated brain regions. We
647 divided the mice into four groups [vehicle + vehicle, vehicle + atomoxetine, DSP-4 (3
648 d) + atomoxetine, DSP-4 (10 d) + atomoxetine; n = 6 in each group]. The specific
649 experimental method followed was as follows. C57BL/6J mice received
650 intraperitoneal injection of DSP-4 (50 mg/kg) or saline (vehicle) 3 days before or 10
651 days before the intraperitoneal injection of atomoxetine (20 mg/kg) or saline (vehicle).
652 One hour later, midazolam was intraperitoneally injected, and the recovery time was
653 recorded. Herein, we verified the physiological effects of DSP-4 using
654 immunohistochemistry.

655 **Effect of intra-LC microinjection of DSP-4 and its interaction with**
656 **intraperitoneal injection of atomoxetine on the recovery time of midazolam**

657 Ten days before the start of this part of the experiment, cannulas were implanted in
658 bilateral LC of C57BL/6J mice using the same method as mentioned above. DSP-4
659 (200 nL, 10 μg/μL) or saline (vehicle) was injected into the LC through these guide
660 cannulas. After 10 days, the mice were intraperitoneally administered atomoxetine or
661 saline (vehicle) 1 h before the intraperitoneal injection of midazolam. The recovery
662 time was recorded for vehicle + vehicle, vehicle + atomoxetine, and DSP-4 +
663 atomoxetine groups (n = 6 mice in each group). Using the same protocol as mentioned
664 above, to complete the experiment, the mice were perfused, and their brains were
665 sectioned. Then, the number of TH+ cells in the DSP-4-treated group and vehicle
666 group were counted and compared individually to investigate the effect of DSP-4
667 microinjection on noradrenergic neurons in bilateral LC.

668 **Effects of lateral ventricle injection and intra-LC microinjection of a GABAA**
669 **receptor antagonist on the recovery time of midazolam**

670 This experiment was performed in the same batch of 8-week-old C57BL/6J mice 1
671 week after lateral ventricle cannula and bilateral LC cannula implantation. Three
672 minutes before the intraperitoneal injection of midazolam, 2000 nL of gabazine (2
673 μg/mL, 4 μg/mL, n = 7, HY-103533, MedChemExpress) was injected into the lateral
674 ventricle cannula or the bilateral cannulas of LC. The recovery time was recorded in
675 each group. During the experiment, the calcium signals were also recorded
676 simultaneously.

677 **Effects of lateral ventricle injection of different adrenoceptor agonists and**
678 **antagonists on the recovery time of midazolam**

679 The experiment was performed in the same batch of 8-week-old C57BL/6J mice 1
680 week after lateral ventricle cannula implantation. The mice were administered
681 agonists or antagonists of different adrenergic receptors through the lateral ventricle.
682 Three minutes before intraperitoneal injection of midazolam, 2000 nL of the α1
683 receptor agonist phenylephrine (10 mg/mL, 20 mg/mL, n = 8, HY-B0471,
684 MedChemExpress) or α1 receptor antagonist prazosin (0.75 mg/mL, 1.5 mg/ml, n = 8,
685 HY-B0193, MedChemExpress) or α2 receptor agonist clonidine (0.75 mg/mL, 1.5
686 mg/mL, n = 9, HY-B0409, MedChemExpress) or α2 receptor yohimbine (15μmol/mL,
687 22.5μmol/mL, 30 μmol/mL, n = 8, Y111137, Aladdin) or β receptor agonist
688 isoprenaline (2 mg/mL, 4 mg/mL, n = 7, I5627, Sigma-Aldrich) or β receptor
689 antagonist propranolol (2·5 mg/mL, 5 mg/mL, n = 6, HY-B0573, MedChemExpress)
690 or vehicle was administered via the lateral ventricle catheter. The recovery time was
691 recorded.

692 To further explore the interaction between the α1 receptor and β receptor, we
693 divided the mice into four groups (vehicle + vehicle, phenylephrine, propranolol, and
694 phenylephrine + propranolol). C57BL/6J mice received intracerebroventricular
695 injection of 2000 nL of phenylephrine (20 mg/kg) or propranolol (5 mg/kg) or
696 phenylephrine (20 mg/kg) + propranolol (5 mg/kg) or vehicle, and 3 min later, they
697 were treated with intraperitoneal injection of midazolam. The recovery time was
698 recorded.

699 **Effects of intra-LC microinjection of GABAA receptor antagonist and**
700 **intra-VLPO microinjection of α1 receptor antagonist on the recovery time of**
701 **midazolam**

702 To investigate the interaction between GABAergic and noradrenergic systems, we
703 divided the mice into four groups (vehicle + vehicle, gabazine + vehicle, vehicle +
704 prazosin, and gabazine + prazosin). The experiment was performed 1 week after LC
705 or VLPO cannula implantation. 200nL of Gabazine, prazosin, or vehicle in the same
706 volume was microinjected into the LC or VLPO through the guide cannula. Three
707 minutes later, the mice were intraperitoneally injected with midazolam. The recovery
708 time was recorded.

709 **EEG recording and analysis**

710 Mice with 2 weeks of viral infection in the target brain area were anesthetized with
711 intraperitoneal injection of 30 mg/kg pentobarbital and fixed on a stereotaxic
712 apparatus to expose the skull for leveling. The top of the head was shaved for all mice,
713 and then the skin was sterilized and dissected to expose the skull. Then, four screws
714 with wires were drilled in the left and right of the fontanelle and in the left and right
715 anterior of the posterior fontanelle, and these were then connected to the head stage
716 where the electroencephalogram (EEG) was recorded. This was followed by dental
717 bone cement stabilization and the application of erythromycin ointment to the
718 operative region. Mice equipped with an EEG head stage were housed individually for
719 one week until they adapted to the recording cable and then moved to the
720 experimental barrel, and the EEG activity of the mice was recorded using the EEG

721 monitor and software.

722 **Immunohistochemistry**

723 For immunohistochemistry analysis of the brain, the mice were euthanized after the
724 experiments, and their brains were carefully extracted from the skull. After perfusion
725 with 4% paraformaldehyde (PFA) in phosphate-buffered saline (PBS), the brains were
726 saturated in 30% sucrose for 24 h. Then, coronal slices (thickness, 35μm) were cut
727 using a freezing microtome (CM30503, Leica Biosystems, Buffalo Grove, IL, USA).
728 Frozen slices were washed three times in PBS for 5 min and incubated in a blocking
729 solution containing 10% normal donkey serum (017-000-121, Jackson Immuno
730 Research, West Grove, PA), 1% bovine serum albumin (A2153, Sigma-Aldrich), and
731 0·3% Triton X-100 in PBS for 2 h at room temperature. The sections were incubated
732 with primary antibodies at 4 ℃ overnight; this was followed by incubation in a
733 solution of secondary antibodies for 2 h at room temperature. The primary antibodies
734 used were rabbit anti-TH (1:1000; AB152, Merck-Millipore), mouse anti-TH (1:1000;
735 MAB318, Merck-Millipore), Mouse anti-GABAA-R(1:500; ab94585, Abcam), and
736 rabbit anti-c-Fos (1:1000, 2250T Rabbit mAb, Cell Signaling Technology, Danvers,
737 Massachusetts, USA), and the secondary antibodies used were donkey anti-rabbit
738 Alexa 546 (1:1000; A10040, Thermo Fisher Scientific), donkey anti-mouse Alexa 546
739 (1:1000; A10036, Thermo Fisher Scientific), Goat anti-rabbit Cy5 (1:1000; A10523,
740 Thermo Fisher Scientific), donkey anti-rabbit Alexa 488 (1:1000; A21206, Thermo
741 Fisher Scientific), and donkey anti-mouse Alexa 488 (1:1000; A21202, Thermo Fisher
742 Scientific). The brain slices were washed three times with PBS for 15 min, and then,

743 they were deposited on glass slides and incubated in a DAPI solution at room
744 temperature for 7 min. Finally, an anti-fluorescence attenuating tablet was applied to
745 seal the slides. Confocal images were acquired using a Nikon A1 laser-scanning
746 confocal microscope (Nikon, Tokyo, Japan), and further image processing was done
747 using ImageJ (NIH, Baltimore, MD).

748 **Statistical analysis**

749 All the experimental data were reported as mean ± SD. GraphPad Prism (GraphPad
750 Software, Inc., San Diego, CA, USA) and SPSS (SPSS Software Inc., Chicago, IL,
751 USA) were used for data visualization and statistical analysis, respectively. Before
752 data analysis, all experimental data were subjected to the Shapiro-Wilk normality test.
753 For comparative analyses of the two groups, if the data were normally distributed,
754 Student's t-test, including independent samples t-test and paired samples t-test, was
755 used. Conversely, if the data were non-normally distributed, the Mann–Whitney U test
756 or Wilcoxon signed-rank test was used. Notably, the Levene test was used to evaluate
757 the homogeneity of variances. After the data met the normal distribution and
758 homogeneity of variances, a one-way analysis of variance followed by Bonferroni's
759 multiple comparison test was used for multiple comparisons. $P < 0.05$ indicated
760 statistical significance.

761 LeYuan Gu[1,2#], WeiHui Shao[2#], Lu Liu[1#], Qing Xu[1#], YuLing Wang[2#], JiaXuan Gu[2#],
762 Yue Yang[2], ZhuoYue Zhang[1], YaXuan Wu[2], Yue Shen[3], Qian Yu[2], XiTing Lian[1],
763 Haixiang Ma[5], YuanLi Zhang[2], HongHai Zhang

764 **Author contributions**

HHZ designed the study. LYG, WHS, LL, QX, YLW, and JXG performed and analyzed most of the experiments. YY, ZYZ, YXW, YS, QY, XTL, and HXM helped with the analysis of experiments. We are grateful to YuDong Zhou and Yi Shen for the experimental design.

Acknowledgments

The work was supported by the National Natural Science Foundation of China (Grant no: 81771403, 81974205), the Natural Science Foundation of Zhejiang Province (LZ20H090001, LHZY24H090003), and the Program of New Century 131 outstanding young talent plan top-level of Hang Zhou to HHZ. We thank YuDong Zhou and Yi Shen for their help in experimental design.

Conflict of interest

The authors declare no conflicts of interest.

Data availability

The data supporting the findings of this study are available within the article upon reasonable request.

References

Arrigoni E, Fuller PM. 2022. The Sleep-Promoting Ventrolateral Preoptic Nucleus: What Have We Learned over the Past 25 Years? *International journal of molecular sciences* **23**. doi:10.3390/ijms23062905

Benarroch EE. 2018. Locus coeruleus. *Cell and tissue research* **373**:221–232. doi:10.1007/s00441-017-2649-1

Berridge CW, Schmeichel BE, España RA. 2012. Noradrenergic modulation of

wakefulness/arousal. *Sleep medicine reviews* **16**:187–97. doi:10.1016/j.smrv.2011.12.003

Brown RE, Basheer R, McKenna JT, Strecker RE, McCarley RW. 2012. Control of sleep and wakefulness. *Physiological reviews* **92**:1087–187. doi:10.1152/physrev.00032.2011

Buysse DJ. 2013. Insomnia. *Jama* **309**:706–16. doi:10.1001/jama.2013.193

Carter ME, Yizhar O, Chikahisa S, Nguyen H, Adamantidis A, Nishino S, Deisseroth K, de Lecea L. 2010. Tuning arousal with optogenetic modulation of locus coeruleus neurons. *Nature neuroscience* **13**:1526–33. doi:10.1038/nn.2682

Chou TC, Bjorkum AA, Gaus SE, Lu J, Scammell TE, Saper CB. 2002. Afferents to the ventrolateral preoptic nucleus. *The Journal of neuroscience : the official journal of the Society for Neuroscience* **22**:977–90. doi:10.1523/jneurosci.22-03-00977.2002

Chung S, Weber F, Zhong P, Tan CL, Nguyen TN, Beier KT, Hörmann N, Chang WC, Zhang Z, Do JP, Yao S, Krashes MJ, Tasic B, Cetin A, Zeng H, Knight ZA, Luo L, Dan Y. 2017. Identification of preoptic sleep neurons using retrograde labelling and gene profiling. *Nature* **545**:477–481. doi:10.1038/nature22350

Citrome L. 2021. Agitation in schizophrenia: origins and evidence-based treatment. *Current opinion in psychiatry* **34**:216–221. doi:10.1097/yco.0000000000000685

Conway A, Rolley J, Sutherland JR. 2016. Midazolam for sedation before procedures. *The Cochrane database of systematic reviews* **2016**:Cd009491. doi:10.1002/14651858.CD009491.pub2

Gebara MA, Siripong N, DiNapoli EA, Maree RD, Germain A, Reynolds CF, Kasckow JW, Weiss PM, Karp JF. 2018. Effect of insomnia treatments on depression: A systematic review and meta-analysis. *Depression and anxiety* **35**:717–731. doi:10.1002/da.22776

Zhou N, Huo F, Yue Y, Yin C. 2020. Specific Fluorescent Probe Based on "Protect-Deprotect" To Visualize the Norepinephrine Signaling Pathway and Drug

Intervention Tracers. J Am Chem Soc. 142(41):17751-17755. doi:10.1021/jacs.0c08956

Han S, Jiang B, Ren J, et al. 2024. Impaired Lactate Release in Dorsal CA1 Astrocytes Contributed to Nociceptive Sensitization and Comorbid Memory Deficits in Rodents. Anesthesiology. 140(3):538-557. doi:10.1097/ALN.0000000000004756

Lian X, Xu Q, Wang Y, et al. 2024. Noradrenergic pathway from the locus coeruleus to heart is implicated in modulating SUDEP. iScience. 2023;26(4):106284. Published 2023 Feb 27. doi:10.1016/j.isci.2023.106284

Li C, Sun T, Zhang Y, et al. 2023. A neural circuit for regulating a behavioral switch in response to prolonged uncontrollability in mice. Neuron. 111(17):2727-2741.e7. doi:10.1016/j.neuron.2023.05.023

Breton-Provencher V, Drummond GT, Feng J, Li Y, Sur M. 2022. Spatiotemporal dynamics of noradrenaline during learned behaviour. Nature. 606(7915):732-738. doi:10.1038/s41586-022-04782-2

Liu Q, Luo X, Liang Z, et al. 2024, Coordination between circadian neural circuit and intracellular molecular clock ensures rhythmic activation of adult neural stem cells. Proc Natl Acad Sci U S A. 121(8):e2318030121. doi:10.1073/pnas.2318030121

Ghit A, Assal D, Al-Shami AS, Hussein DEE. 2021. GABA(A) receptors: structure, function, pharmacology, and related disorders. *Journal, genetic engineering & biotechnology* **19**:123. doi:10.1186/s43141-021-00224-0

Hayat H, Regev N, Matosevich N, Sales A, Paredes-Rodriguez E, Krom AJ, Bergman L, Li Y, Lavigne M, Kremer EJ, Yizhar O, Pickering AE, Nir Y. 2020. Locus coeruleus norepinephrine activity mediates sensory-evoked awakenings from sleep. *Science advances* **6**:eaaz4232. doi:10.1126/sciadv.aaz4232

Kanto JH. 1985. Midazolam: the first water-soluble benzodiazepine. Pharmacology, pharmacokinetics and efficacy in insomnia and anesthesia. *Pharmacotherapy* **5**:138–55. doi:10.1002/j.1875-9114.1985.tb03411.x

Kim HK, Leonard JB, Corwell BN, Connors NJ. 2021. Safety and efficacy of pharmacologic agents used for rapid tranquilization of emergency department patients with acute agitation or excited delirium. *Expert opinion on drug safety* **20**:123–138.

852 doi:10.1080/14740338.2021.1865911

853 Lee SH, Dan Y. 2012. Neuromodulation of brain states. *Neuron* **76**:209–22.
854 doi:10.1016/j.neuron.2012.09.012

855 Liang Y, Shi W, Xiang A, Hu D, Wang L, Zhang L. 2021. The NAergic locus
856 coeruleus-ventrolateral preoptic area neural circuit mediates rapid arousal from sleep.
857 *Current biology : CB* **31**:3729-3742.e5. doi:10.1016/j.cub.2021.06.031

858 Mandrioli R, Mercolini L, Raggi MA. 2008. Benzodiazepine metabolism: an
859 analytical perspective. *Current drug metabolism* **9**:827–44.
860 doi:10.2174/138920008786049258

861 Maramai S, Benchekroun M, Ward SE, Atack JR. 2020. Subtype Selective
862 γ-Aminobutyric Acid Type A Receptor (GABA(A)R) Modulators Acting at the
863 Benzodiazepine Binding Site: An Update. *Journal of medicinal chemistry*
864 **63**:3425–3446. doi:10.1021/acs.jmedchem.9b01312

865 Massimini M, Ferrarelli F, Sarasso S, Tononi G. 2012. Cortical mechanisms of loss of
866 consciousness: insight from TMS/EEG studies. *Archives italiennes de biologie*
867 **150**:44–55. doi:10.4449/aib.v150i2.1361

868 Nelson LE, Lu J, Guo T, Saper CB, Franks NP, Maze M. 2003. The
869 alpha2-adrenoceptor agonist dexmedetomidine converges on an endogenous
870 sleep-promoting pathway to exert its sedative effects. *Anesthesiology* **98**:428–36.
871 doi:10.1097/00000542-200302000-00024

872 Nordt SP, Clark RF. 1997. Midazolam: a review of therapeutic uses and toxicity. *The*
873 *Journal of emergency medicine* **15**:357–65. doi:10.1016/s0736-4679(97)00022-x

874 Olkkola KT, Ahonen J. 2008. Midazolam and other benzodiazepines. *Handbook of*
875 *experimental pharmacology* 335–60. doi:10.1007/978-3-540-74806-9_16

876 Olsen RW. 2018. GABA(A) receptor: Positive and negative allosteric modulators.
877 *Neuropharmacology* **136**:10–22. doi:10.1016/j.neuropharm.2018.01.036

878 Perlis ML, Posner D, Riemann D, Bastien CH, Teel J, Thase M. 2022. Insomnia.
879 *Lancet (London, England)* **400**:1047–1060. doi:10.1016/s0140-6736(22)00879-0

880 Poe GR, Foote S, Eschenko O, Johansen JP, Bouret S, Aston-Jones G, Harley CW,
881 Manahan-Vaughan D, Weinshenker D, Valentino R, Berridge C, Chandler DJ,
882 Waterhouse B, Sara SJ. 2020. Locus coeruleus: a new look at the blue spot. *Nature*
883 *reviews Neuroscience* **21**:644–659. doi:10.1038/s41583-020-0360-9

884 Quinlan JJ, Homanics GE, Firestone LL. 1998. Anesthesia sensitivity in mice that
885 lack the beta3 subunit of the gamma-aminobutyric acid type A receptor.
886 *Anesthesiology* **88**:775–80. doi:10.1097/00000542-199803000-00030

887 Reves JG, Fragen RJ, Vinik HR, Greenblatt DJ. 1985. Midazolam: pharmacology and
888 uses. *Anesthesiology* **62**:310–24.

889 Riemann D, Nissen C, Palagini L, Otte A, Perlis ML, Spiegelhalder K. 2015. The
890 neurobiology, investigation, and treatment of chronic insomnia. *The Lancet Neurology*
891 **14**:547–58. doi:10.1016/s1474-4422(15)00021-6

892 Saper CB, Scammell TE, Lu J. 2005. Hypothalamic regulation of sleep and circadian
893 rhythms. *Nature* **437**:1257–63. doi:10.1038/nature04284

894 Shafer A. 1998. Complications of sedation with midazolam in the intensive care unit
895 and a comparison with other sedative regimens. *Critical care medicine* **26**:947–56.
896 doi:10.1097/00003246-199805000-00034

897 Shehabi Y, Bellomo R, Reade MC, Bailey M, Bass F, Howe B, McArthur C, Seppelt
898 IM, Webb S, Weisbrodt L. 2012. Early intensive care sedation predicts long-term
899 mortality in ventilated critically ill patients. *American journal of respiratory and*
900 *critical care medicine* **186**:724–31. doi:10.1164/rccm.201203-0522OC

901 Sherin JE, Elmquist JK, Torrealba F, Saper CB. 1998. Innervation of histaminergic
902 tuberomammillary neurons by GABAergic and galaninergic neurons in the
903 ventrolateral preoptic nucleus of the rat. *The Journal of neuroscience : the official*
904 *journal of the Society for Neuroscience* **18**:4705–21.

905 doi:10.1523/jneurosci.18-12-04705.1998

906 Sherin JE, Shiromani PJ, McCarley RW, Saper CB. 1996. Activation of ventrolateral
907 preoptic neurons during sleep. *Science (New York, NY)* **271**:216–9.
908 doi:10.1126/science.271.5246.216

909 Sigel E, Ernst M. 2018. The Benzodiazepine Binding Sites of GABA(A) Receptors.
910 *Trends in pharmacological sciences* **39**:659–671. doi:10.1016/j.tips.2018.03.006

911 Smith R, Brown J. 2017. Midazolam for status epilepticus. *Australian prescriber*
912 **40**:23–25. doi:10.18773/austprescr.2017.005

913 Suárez-Pereira I, Llorca-Torralba M, Bravo L, Camarena-Delgado C, Soriano-Mas C,
914 Berrocoso E. 2022. The Role of the Locus Coeruleus in Pain and Associated
915 Stress-Related Disorders. *Biological psychiatry* **91**:786–797.
916 doi:10.1016/j.biopsych.2021.11.023

917 Sutton EL. 2021. Insomnia. *Annals of internal medicine* **174**:Itc33-itc48.
918 doi:10.7326/aitc202103160

919 Van Egroo M, Koshmanova E, Vandewalle G, Jacobs HIL. 2022. Importance of the
920 locus coeruleus-norepinephrine system in sleep-wake regulation: Implications for
921 aging and Alzheimer's disease. *Sleep medicine reviews* **62**:101592.
922 doi:10.1016/j.smrv.2022.101592

923 Vanini G, Bassana M, Mast M, Mondino A, Cerda I, Phyle M, Chen V, Colmenero AV,
924 Hambrecht-Wiedbusch VS, Mashour GA. 2020. Activation of Preoptic GABAergic or
925 Glutamatergic Neurons Modulates Sleep-Wake Architecture, but Not Anesthetic State
926 Transitions. *Current biology : CB* **30**:779-787.e4. doi:10.1016/j.cub.2019.12.063

927 Nguyen, G., & Postnova, S. 2021. Progress in modelling of brain dynamics during
928 anaesthesia and the role of sleep-wake circuitry. Biochemical pharmacology, 191,
929 114388. https://doi.org/10.1016/j.bcp.2020.114388

FIGURE LEGENDS

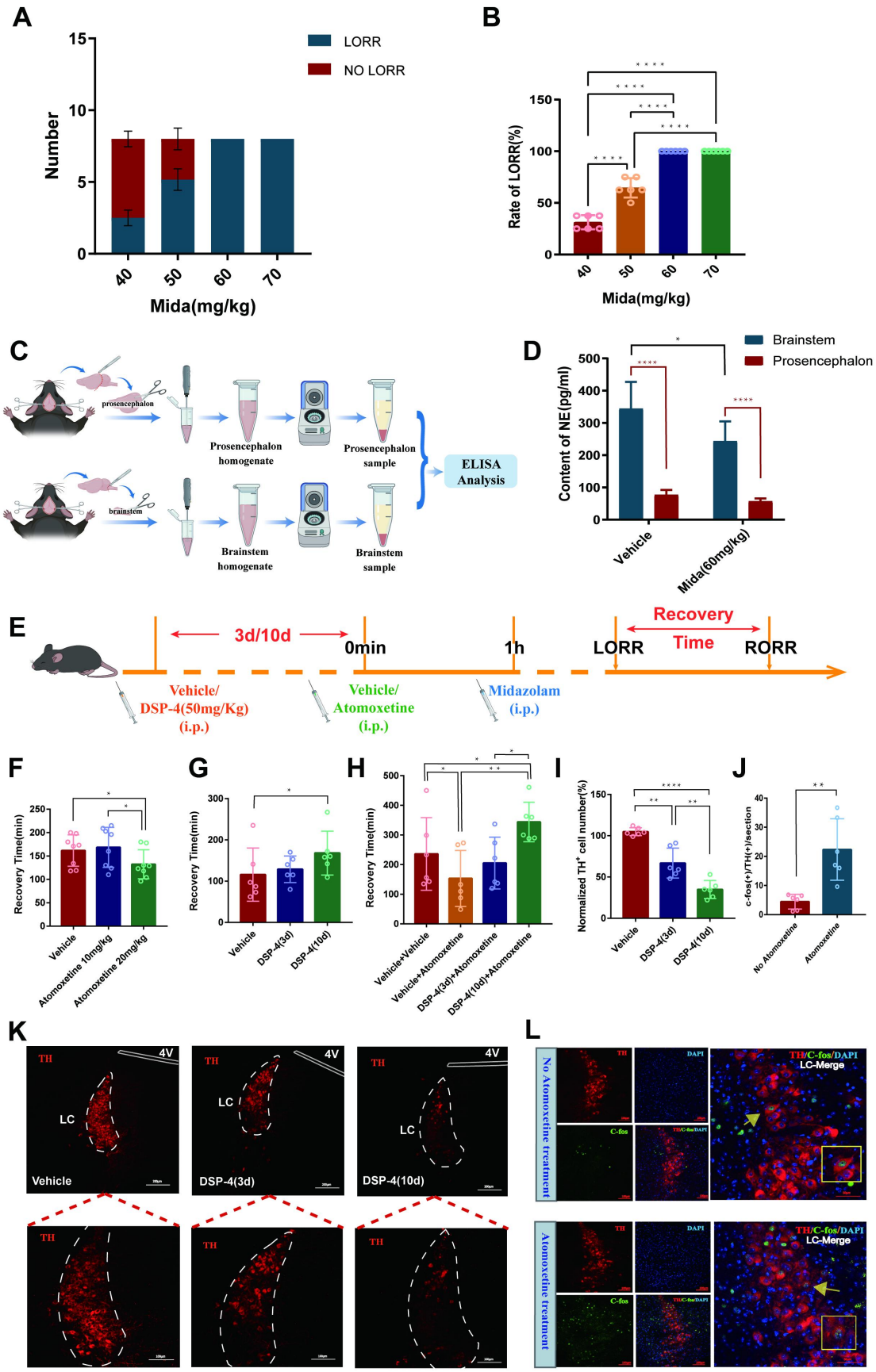

931 **Figure 1. The noradrenergic system is involved in recovery from midazolam**
932 **administration.**
933 **(A)** Number of LORR and no LORR induced by different doses of midazolam in
934 C57BL/6J mice.
935 **(B)** Rate of LORR (%) in C57BL/6J mice at different doses of midazolam.
936 **(C)** Protocol for investigating changes in the content of NE in the prosencephalon and
937 brainstem of C57BL/6J mice by ELISA.
938 **(D)** Content of NE in the prosencephalon and brainstem in the vehicle and midazolam
939 (60mg/Kg, i.p.) groups.
940 **(E)** Protocol for exploring the influence of intraperitoneal injection of DSP-4 on the
941 atomoxetine-mediated shortening of the recovery time from midazolam
942 administration.
943 **(F)** Comparison of recovery time in the vehicle, Atomoxitine (10mg/Kg, i.p.), and
944 Atomoxitine (20mg/Kg, i.p.) groups.
945 **(G)** Comparison of recovery time in the vehicle, DSP-4 (50 mg/kg, 3 days before, i.p.),
946 and DSP-4 (50 mg/kg, 10 days before, i.p.) groups.
947 **(H)** Comparison of recovery time in the vehicle + vehicle, vehicle + Atomoxitine,
948 DSP-4 (3 days before) + Atomoxitine, and DSP-4(10 days before) + Atomoxitine
949 groups.
950 **(I)** Comparison of normalized TH (+) cell number in the LC in the vehicle, DSP-4 (3
951 days before), and DSP-4(10 days before).
952 **(J)** The quantification of c-Fos (+)/TH (+) cells with or without intraperitoneal
953 injection of atomoxetine.
954 **(K)** Images of TH+ neurons in the LC after intraperitoneal injection of vehicle, DSP-4
955 (3 days), or DSP-4 (10 days) (panels on the lower show magnified images of the
956 panels on the upper).
957 **(L)** Representative images showing the changes in TH (+) neuronal activity with or
958 without intraperitoneal injection of atomoxetine.
959 Mida: midazolam; NE: norepinephrine; i.p.: intraperitoneal injection; LORR: loss of
960 righting reflex; RORR: recovery of righting reflex; LC: locus coeruleus; TH: tyrosine

hydroxylase; *p<0.05; **p<0.01; ***p<0.001; ****p<0.0001

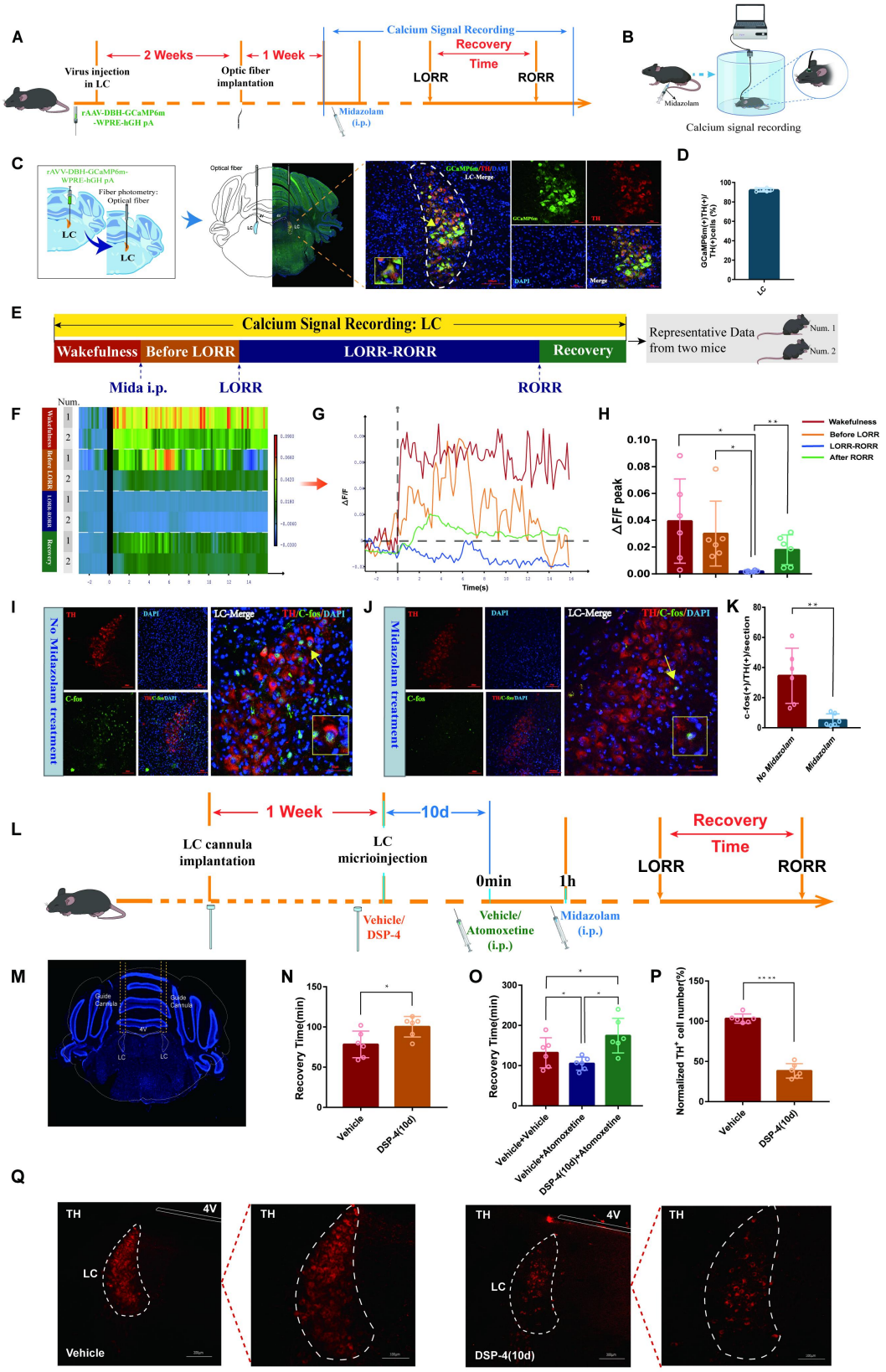

Figure 2. LC^{NE} neuronal activity is significantly reduced after midazolam administration and selective ablation of LCNE neurons hinders recovery from

964 **midazolam**

965 **(A)** A schematic of the fiber optic recording of calcium signal in the LC.

966 **(B)** A schematic of the calcium signaling recording device.

967 **(C)** A representative photomicrograph showing the microinjection and optical fiber
968 locations and the co-expression of GCaMP6s and TH.

969 **(D)** Quantification of the percentage of GCaMP6m (+)/TH (+) colocalization in all
970 TH (+) neurons in LC.

971 **(E)** Schematic diagram of the method of dividing the entire recording of the calcium
972 signal at the LC into four stages, and sources of heatmap and ΔF/F(%) statistical data.
973 (The time points for awake, midazolam injection, LORR and RORR in mice were
974 respectively selected as time=0.The selected traces lasting for 20s was based on the
975 length of a complete Ca2+ signal)

976 **(F)** A heatmap of calcium signaling changes in bilateral LC^{NE} neurons induced by
977 midazolam. (Two representative mice were selected for the fiber optic recording of
978 calcium signals, and the whole recording was divided into four stages, each stage as a
979 group for statistical analysis of calcium signaling).

980 **(G)** A statistical diagram of calcium signaling changes in bilateral LC^{NE} neurons
981 induced by midazolam.

982 **(H)** The peak ΔF/F in the wakefulness, before LORR, LORR-RORR, and after RORR
983 stages.

984 **(I-J)** Representative images showing the co-expression of c-Fos and TH in the LC
985 without or with midazolam treatment.

986 **(K)** The quantification of c-Fos (+)/TH (+) cells in the LC with midazolam or without
987 midazolam treatment.

988 **(L)** Protocol for exploring the influence of intra-LC microinjection DSP-4 on the
989 atomoxetine-mediated shortening of the recovery time from midazolam
990 administration.

991 **(M)** The representative photomicrograph shows the tracks of cannulas implanted into
992 bilateral LC.

993 **(N)** Results showed the effects of microinjection of DSP-4 (10 days before) into

994 bilateral LC on the recovery time of midazolam.

995 **(O)** Results showed the effects of vehicle + vehicle, vehicle + atomoxetine, and
996 DSP-4 (10 days before) + atomoxetine on the recovery time of midazolam.

997 **(P)** Comparison of normalized TH (+) cell number in the LC with or without DSP-4
998 (10 days before) microinjected in the bilateral LC.

999 **(Q)** Images of TH+ neurons in the LC after microinjection of DSP-4 or vehicle for 10
1000 days (panels on the right show magnified images of the panels on the left).

1001 LC: locus coeruleus; i.p.: intraperitoneal injection; LORR: loss of righting reflex;
1002 RORR: recovery of righting reflex; TH: tyrosine hydroxylase; *$p<0.05$; **$p<0.01$;
1003 ****$p<0.0001$

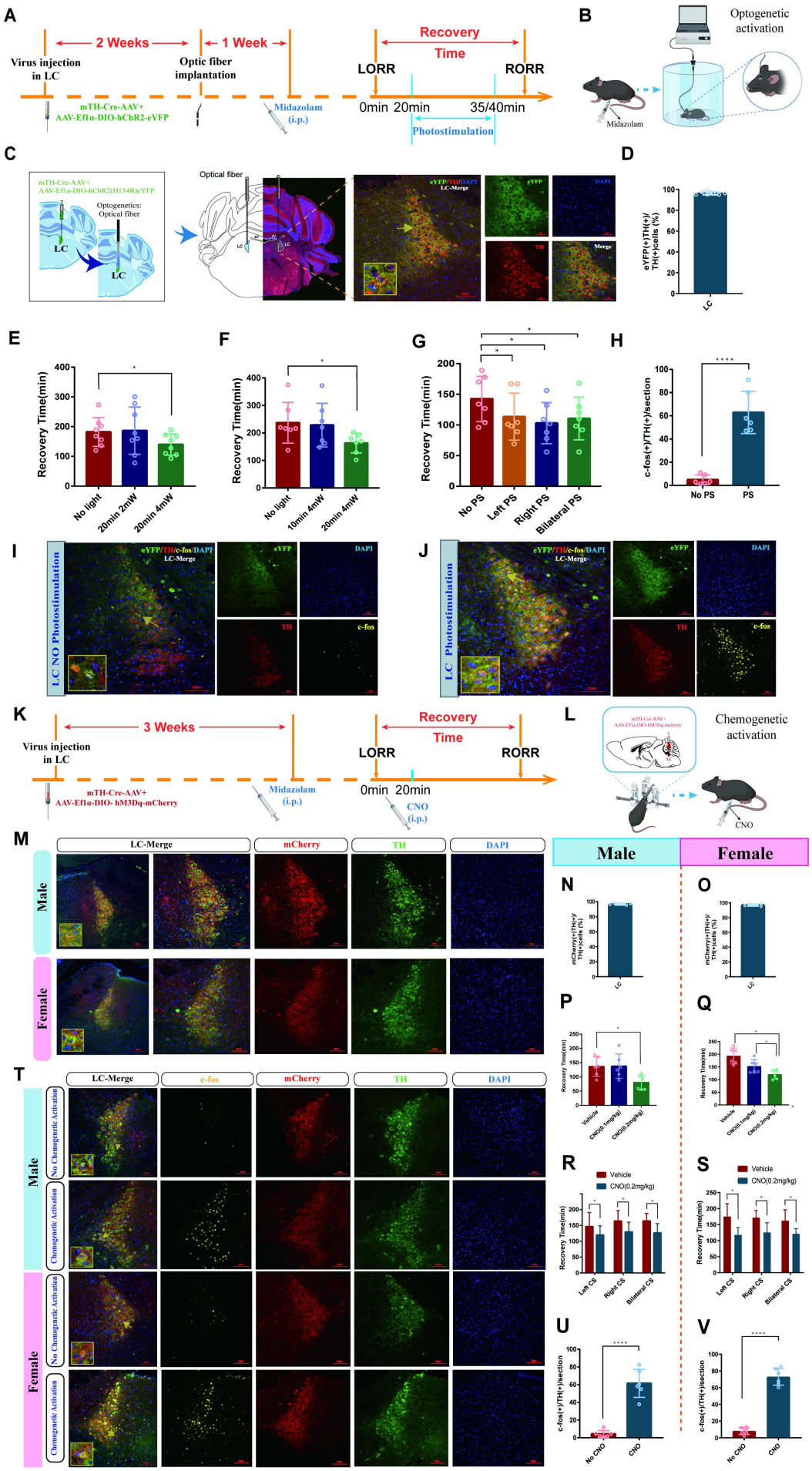
A
2 Weeks
1 Week
Virus injection in LC
Optic fiber implantation
mTH-Cre-AAV+
AAV-Ef1α-DIO-hChR2-eYFP
Midazolam (i.p.)
Recovery Time
LORR
RORR
0min 20min
35/40min
Photostimulation
B
Optogenetic activation
Midazolam
C
Optical fiber
LC
D
E
Recovery Time(min)
No light
20min 2mW
20min 4mW
F
10min 4mW
G
No PS
Left PS
Right PS
Bilateral PS
H
c-fos(+)/TH(+)/section
PS
I
LC NO Photostimulation
eYFP/TH/c-fos/DAPI
LC-Merge
eYFP
DAPI
TH
c-fos
J
LC Photostimulation
K
3 Weeks
mTH-Cre-AAV+
AAV-Ef1α-DIO- hM3Dq-mCherry
CNO (i.p.)
L
Chemogenetic activation
CNO
M
LC-Merge
mCherry
TH
DAPI
Male
Female
N
O
P
Q
R
S
Vehicle
CNO(0.2mg/kg)
Left CS
Right CS
Bilateral CS
T
c-fos
No Chemogenetic Activation
Chemogenetic Activation
U
V
No CNO
CNO

1005 **Figure 3. Optogenetic or chemogenetic activation of LC^{NE} neurons promotes**
1006 **recovery from midazolam**
1007 **(A)** Protocol for the effect of photostimulation of LC^{NE} neurons with different light
1008 parameters on the recovery time of midazolam.
1009 **(B)** A schematic of the optogenetic instrument.
1010 **(C)** A representative photomicrograph showing the locations of optical fiber and virus
1011 expression and the co-expression of hChR2 and TH.
1012 **(D)** Quantification of the percentage of eYFP (+)/TH (+) colocalization in all TH (+)
1013 neurons in LC.
1014 **(E-F)** Results showed the effect of photostimulation of LC^{NE} neurons with different
1015 light parameters on the recovery time of midazolam.
1016 **(G)** Results showed the effect of left, right, and bilateral photostimulation of the LC^{NE}
1017 neurons on the recovery time of midazolam.
1018 **(H)** The quantification of c-Fos (+)/TH (+) cells in the LC with or without
1019 photostimulation.
1020 **(I-J)** Representative images showing the co-expression of c-Fos and TH cells in the
1021 LC with or without photostimulation.
1022 **(K-L)** Protocol and instrument for the effect of chemogenetic activation of LC^{NE}
1023 neurons on the recovery time of midazolam.
1024 **(M)** A representative photomicrograph showing the virus expression and the
1025 co-expression of mCherry and TH in the LC of male and female mice.
1026 **(N-O)** Quantification of the percentage of mCherry (+)/TH (+) colocalization in all
1027 TH (+) neurons in LC.
1028 **(P-Q)** Results showed the effect of chemogenetic activation of LC^{NE} neurons with
1029 different doses of CNO (i.p.) on the recovery time of midazolam in male and female
1030 mice.
1031 **(R-S)** Results showed the effect of left, right, and bilateral chemogenetic activation of
1032 the LC^{NE} neurons on the recovery time of midazolam in male and female mice.
1033 **(T)** Representative images showing the co-expression of c-Fos and TH cells in the LC
1034 of male and female mice with or without intraperitoneal injection of CNO (0.2

1035 mg/kg).

1036 **(U-V)** The quantification of c-Fos (+)/TH (+) cells in the LC with or without

1037 chemogenetic stimulation.

1038 LC: locus coeruleus; i.p.: intraperitoneal injection; LORR: loss of righting reflex;

1039 RORR: recovery of righting reflex; TH: tyrosine hydroxylase; PS: photostimulation;

1040 CS: chemogenetic stimulation; *$p<0.05$; ****$p<0.0001$

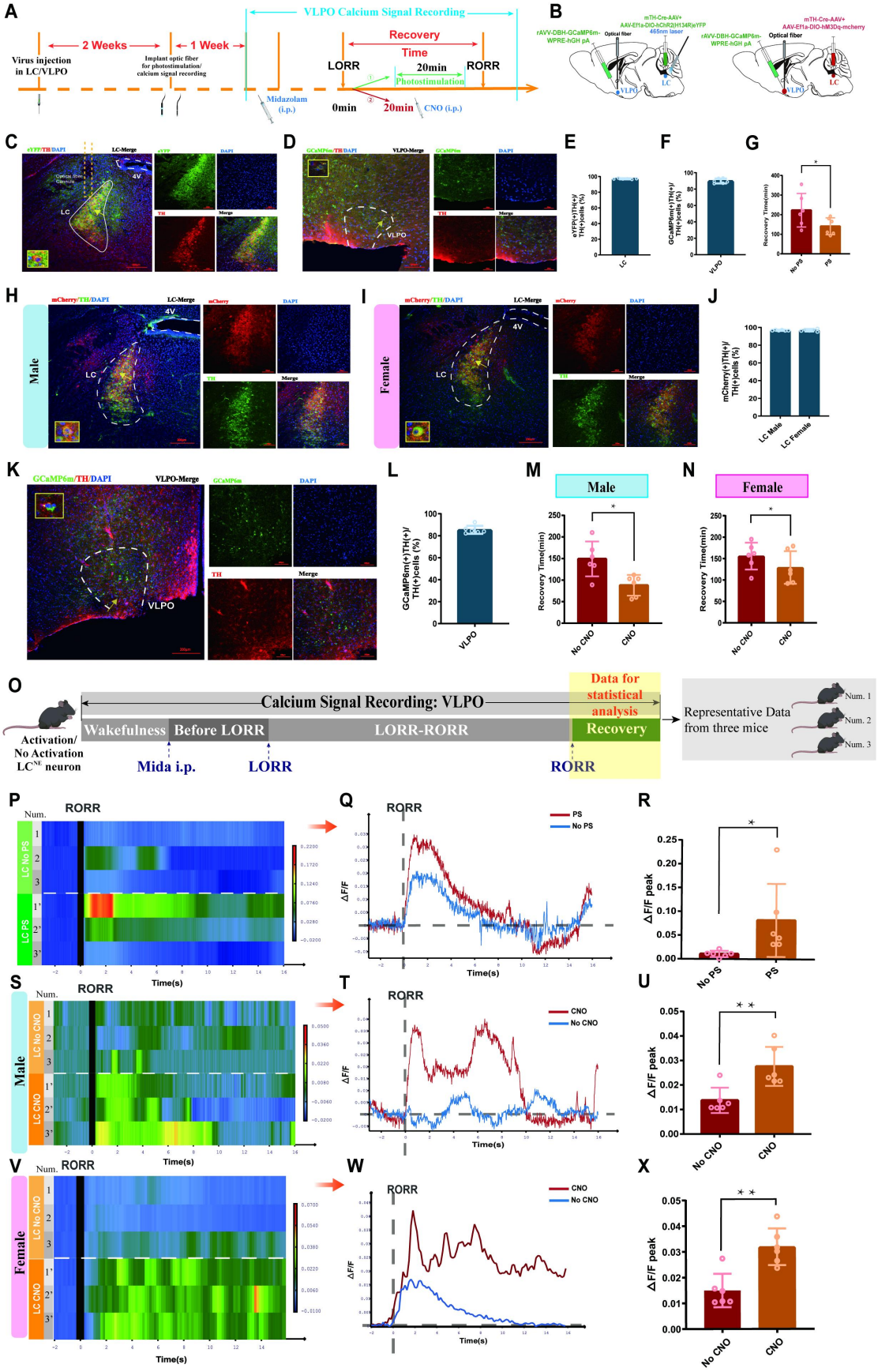
A
VLPO Calcium Signal Recording
2 Weeks
1 Week
Virus injection in LC/VLPO
Implant optic fiber for photostimulation/ calcium signal recording
Recovery Time
LORR
20min
RORR
Photostimulation
Midazolam (i.p.)
0min
20min
CNO (i.p.)
B
rAVV-DBH-GCaMP6m-WPRE-hGH pA
Optical fiber
mTH-Cre-AAV+ AAV-Ef1a-DIO-hChR2(H134R)eYFP
465nm laser
VLPO
LC
rAVV-DBH-GCaMP6m-WPRE-hGH pA
mTH-Cre-AAV+ AAV-Ef1a-DIO-hM3Dq-mcherry
C
D
E
F
G
H
Male
I
Female
J
LC Male
LC Female
K
L
M
Male
N
Female
No CNO
CNO
O
Activation/ No Activation LC^NE neuron
Calcium Signal Recording: VLPO
Data for statistical analysis
Wakefulness
Before LORR
LORR-RORR
Recovery
Mida i.p.
LORR
RORR
Representative Data from three mice
Num. 1
Num. 2
Num. 3
P
RORR
LC No PS
LC PS
Time(s)
Q
PS
No PS
ΔF/F
R
ΔF/F peak
S
Male
LC No CNO
LC CNO
T
CNO
No CNO
U
V
Female
W
X

1042 **Figure 4. LC-VLPO NEergic neural circuit was involved in the recovery from**
1043 **midazolam**
1044 **(A)** Protocol for optogenetic or chemogenetic activation of LC^{NE} neurons and
1045 recording of calcium signaling changes in VLPO.
1046 **(B)** A schematic of the location of optogenetic or chemogenetic virus injection site in
1047 the LC and calcium signaling recording virus injection site in the VLPO.
1048 **(C)** A representative image showing the co-expression of hChR2 and TH in the LC.
1049 **(D)** A representative image showing the co-expression of GCaMP6s and TH in the
1050 VLPO in male mice.
1051 **(E)** Quantification of the percentage of eYFP (+)/TH (+) colocalization in all TH (+)
1052 neurons in LC.
1053 **(F)** Quantification of the percentage of GCaMP6m (+)/TH (+) colocalization in all TH
1054 (+) neurons in VLPO.
1055 **(G)** Results showed the effects of optogenetic activation of LC^{NE} neurons on the
1056 recovery time of midazolam.
1057 **(H-I)** A representative image showing the co-expression of hM3Dq and TH in the LC
1058 of male and female mice.
1059 **(J)** Quantification of the percentage of mCherry (+)/TH (+) colocalization in all TH (+)
1060 neurons in LC.
1061 **(K)** A representative image showing the co-expression of GCaMP6s and TH in the
1062 VLPO in female mice.
1063 **(L)** Quantification of the percentage of GCaMP6m (+)/TH (+) colocalization in all
1064 TH (+) neurons in VLPO
1065 **(M-N)** Results showed the effects of chemogenetic activation of LC^{NE} neurons on the
1066 recovery time of midazolam in male and female mice.
1067 **(O)** Schematic diagram of the method of recording the calcium signal at the VLPO,
1068 and sources of statistical data.
1069 **(P-Q)** Heatmap and statistical diagram of calcium signaling changes in bilateral
1070 VLPO at the after RORR stage with or without optogenetic activation of LC^{NE}
1071 neurons. (Showing changes in calcium signaling during the RORR and the Recovery

period; optogenetic activation group, n=3; no optogenetic activation group, n=3) (The time points for RORR in mice were respectively selected as time=0.The selected traces lasting for 20s was based on the length of a complete Ca2+ signal)

(R) The peak ΔF/F in the VLPO with or without activation of LC^{NE} neurons using optogenetics.

(S-T, V-W) Heatmap and statistical diagram of calcium signaling changes in bilateral VLPO at the after RORR stage with or without chemogenetic activation of LC^{NE} neurons in male and female mice. (Showing changes in calcium signaling during the RORR and the Recovery period; chemogenetic activation group, n=3; no chemogenetic activation group, n=3)

(U, X) The peak ΔF/F in the VLPO with or without activation of LC^{NE} neurons using chemogenetics in male and female mice.

LC: locus coeruleus; VLPO: ventrolateral preoptic nucleus; i.p.: intraperitoneal injection; LORR: loss of righting reflex; RORR: recovery of righting reflex; TH: tyrosine hydroxylase; PS: photostimulation; *p<0.05; **p<0.

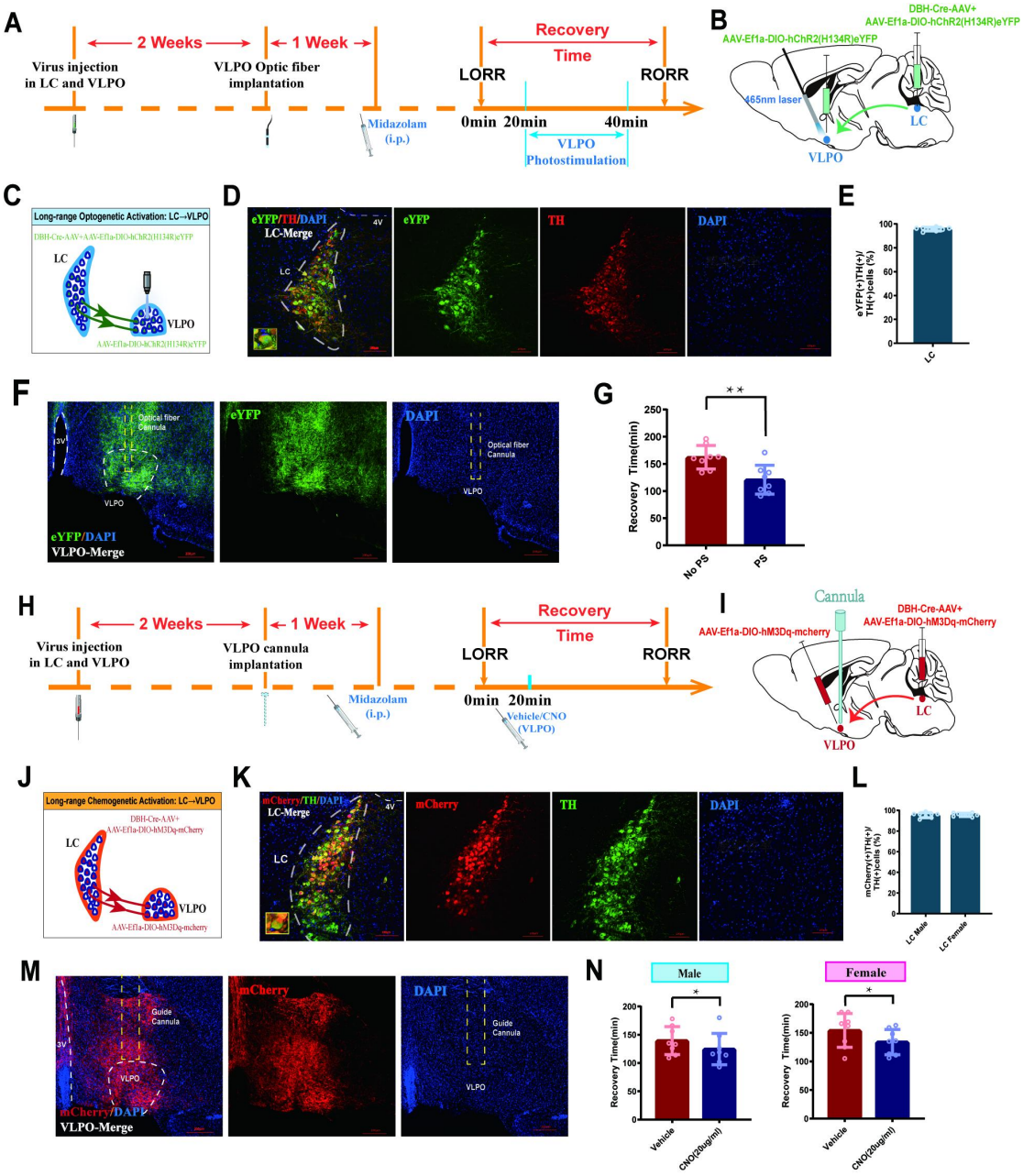

Figure 5. Activation of LC-VLPO NEergic neural circuit promotes recovery from midazolam

(A) Protocol for intra-LC/VLPO microinjection of the virus and optogenetic activation of VLPO.

(B-C) Schematic of LC–VLPO long-range optogenetic activation and the location of optogenetic virus microinjection and optic fiber implantation.

(D) Representative images showing the co-expression of hChR2 and TH in the LC.

(E) Quantification of the percentage of eYFP (+)/TH (+) colocalization in all TH (+) neurons in LC.

1097 **(F)** Distributions of hChR2-eYFP terminals from LC-NA neurons and DAPI labeling
1098 in the VLPO.
1099 **(G)** Result showed the effect of LC–VLPO long-range optogenetic activation on the
1100 recovery time of midazolam.
1101 **(H)** Protocol for intra-LC/VLPO microinjection of the virus and chemogenetic
1102 activation of VLPO.
1103 **(I-J**) Schematic of LC–VLPO long-range chemogenetic activation and the location of
1104 chemogenetic virus microinjection and cannula implantation.
1105 **(K)** Representative images showing the co-expression of mCherry and TH in the LC.
1106 **(L)** Quantification of the percentage of mCherry (+)/TH (+) colocalization in all TH
1107 (+) neurons in LC.
1108 **(M)** Distributions of hM3Dq-mCherry terminals from LC-NA neurons and DAPI
1109 labeling in the VLPO.
1110 **(N)** Result showed the effect of LC–VLPO long-range chemogenetic activation on the
1111 recovery time of midazolam in male and female mice.
1112 LC: locus coeruleus; VLPO: ventrolateral preoptic nucleus; i.p.: intraperitoneal
1113 injection; LORR: loss of righting reflex; RORR: recovery of righting reflex; TH:
1114 tyrosine hydroxylase; PS: photostimulation; *$p<0.05$; **$p<0.01$

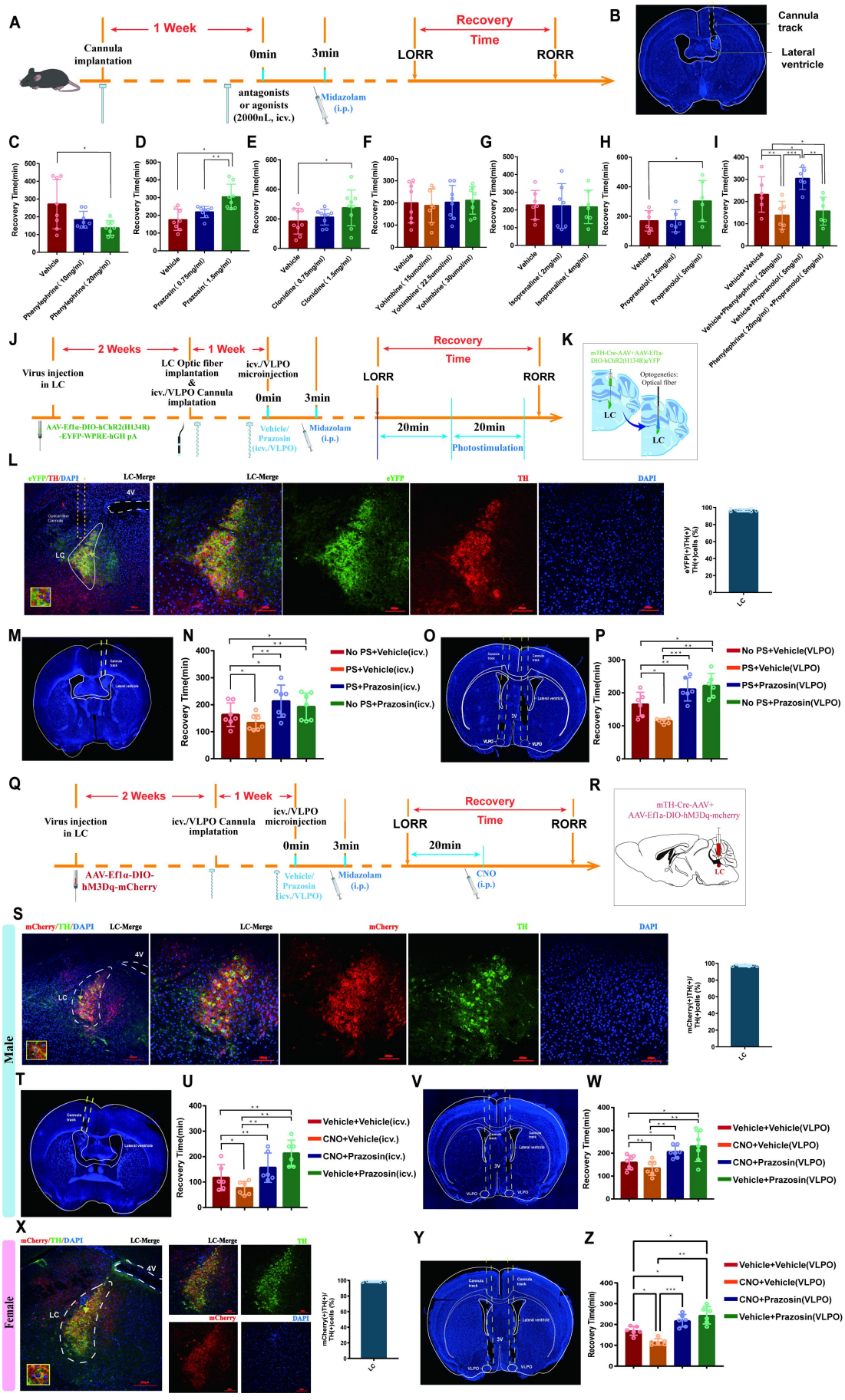
A
1 Week
Cannula implantation
0min
3min
LORR
Recovery Time
RORR
antagonists or agonists (2000nL, icv.)
Midazolam (i.p.)
B
Cannula track
Lateral ventricle
C
D
E
F
G
H
I
Recovery Time(min)
Vehicle
Phenylephrine (10mg/ml)
Phenylephrine (20mg/ml)
Prazosin (0.75mg/ml)
Prazosin (1.5mg/ml)
Clonidine (0.75mg/ml)
Clonidine (1.5mg/ml)
Yohimbine (15umol/ml)
Yohimbine (22.5umol/ml)
Yohimbine (30umol/ml)
Isoprenaline (2mg/ml)
Isoprenaline (4mg/ml)
Propranolol (2.5mg/ml)
Propranolol (5mg/ml)
Vehicle+Vehicle
Vehicle+Phenylephrine (20mg/ml)
Vehicle+Propranolol (5mg/ml)
Phenylephrine (20mg/ml) +Propranolol (5mg/ml)
J
2 Weeks
1 Week
Virus injection in LC
LC Optic fiber implantation & icv./VLPO Cannula implatation
icv./VLPO microinjection
0min
3min
LORR
Recovery Time
RORR
AAV-Ef1α-DIO-hChR2(H134R) -EYFP-WPRE-hGH pA
Vehicle/ Prazosin (icv./VLPO)
Midazolam (i.p.)
20min
20min
Photostimulation
K
mTH-Cre-AAV+AAV-Ef1a-DIO-hChR2(H134R)eYFP
Optogenetics: Optical fiber
LC
L
eYFP/TH/DAPI
LC-Merge
eYFP
TH
DAPI
4V
LC
eYFP(+)TH(+)/ TH(+)cells (%)
M
N
O
P
Recovery Time(min)
No PS+Vehicle(icv.)
PS+Vehicle(icv.)
PS+Prazosin(icv.)
No PS+Prazosin(icv.)
No PS+Vehicle(VLPO)
PS+Vehicle(VLPO)
PS+Prazosin(VLPO)
No PS+Prazosin(VLPO)
Q
2 Weeks
1 Week
Virus injection in LC
icv./VLPO Cannula implatation
icv./VLPO microinjection
0min
3min
LORR
Recovery Time
RORR
20min
AAV-Ef1α-DIO-hM3Dq-mCherry
Vehicle/ Prazosin (icv./VLPO)
Midazolam (i.p.)
CNO (i.p.)
R
mTH-Cre-AAV+ AAV-Ef1a-DIO-hM3Dq-mcherry
LC
S
Male
mCherry/TH/DAPI
LC-Merge
mCherry
TH
DAPI
4V
LC
mCherry(+)TH(+)/ TH(+)cells (%)
T
U
V
W
Vehicle+Vehicle(icv.)
CNO+Vehicle(icv.)
CNO+Prazosin(icv.)
Vehicle+Prazosin(icv.)
Vehicle+Vehicle(VLPO)
CNO+Vehicle(VLPO)
CNO+Prazosin(VLPO)
Vehicle+Prazosin(VLPO)
X
Female
Y
Z

1115

1116 **Figure 6. ICV injection or intra-VLPO microinjection of α1-R antagonist**
1117 **reverses the pro-recovery effect of optogenetic or chemogenetic of activation**
1118 **LC^{NE} neurons**
1119 **(A)** A schematic of intracerebroventricular injection of different noradrenergic
1120 receptor agonists and antagonists.
1121 **(B)** A representative photomicrograph showing the tracks of cannulas implanted into
1122 the lateral ventricle.
1123 **(C-H)** Results showed the effects of intracerebroventricular injection of different
1124 doses of phenylephrine, prazosin, clonidine, yohimbine, isoprenaline, and propranolol
1125 on the recovery time of midazolam.
1126 **(I)** Results showed the effects of intracerebroventricular injection of phenylephrine
1127 (20mg/mL) and different doses of propranolol on the recovery time of midazolam.
1128 **(J)** Protocol for photostimulation of LC^{NE} neurons and intracerebroventricular
1129 injection or intra-VLPO microinjection of α1-R antagonist.
1130 **(K)** Schematic of the brief process of optogenetic activation.
1131 **(L)** The representative photomicrograph showing microinjection and optical fiber
1132 locations of the co-expression of hChR2 and TH in the LC. Moreover, quantification
1133 of the percentage of eYFP (+)/TH (+) colocalization in all TH (+) neurons in LC have
1134 been showed.
1135 **(M, O)** A representative photomicrograph showing the tracks of cannulas implanted
1136 into the lateral ventricle and bilateral VLPO.
1137 **(N, P)** Results showed the effects of photostimulation of LC^{NE} neurons and
1138 intracerebroventricular injection or intra-VLPO microinjection of prazosin on the
1139 recovery time of midazolam.
1140 **(Q)** Protocol for chemogenetic activation of LC^{NE} neurons and intracerebroventricular
1141 injection or intra-VLPO microinjection of an α1-R antagonist.
1142 **(R)** Schematic of the location of virus injection.
1143 **(S)** The representative photomicrograph showing the co-expression of hM3Dq and
1144 TH in the LC of male mice. Moreover, quantification of the percentage of mCherry
1145 (+)/TH (+) colocalization in all TH (+) neurons in LC have been showed.
1146 **(T, V)** A representative photomicrograph showing the tracks of cannulas implanted

1147 into the lateral ventricle and bilateral VLPO in the male mice.

1148 **(U, W)** Results showed the effects of chemogenetic activation of LC^{NE} neurons and
1149 intracerebroventricular injection or intra-VLPO microinjection of prazosin on the
1150 recovery time of midazolam in male mice.

1151 **(X)** A representative photomicrograph showing the co-expression of hM3Dq and TH
1152 in the LC. Moreover, quantification of the percentage of mCherry (+)/TH (+)
1153 colocalization in all TH (+) neurons in LC have been showed.

1154 **(Y)** The tracks of cannulas implanted into the bilateral VLPO in the female mice.

1155 **(Z)** Results showed the effects of chemogenetic activation of LC^{NE} neurons and
1156 intra-VLPO microinjection of prazosin on the recovery time of midazolam in female
1157 mice.

1158 LC: locus coeruleus; VLPO: ventrolateral preoptic nucleus; i.p.: intraperitoneal
1159 injection; LORR: loss of righting reflex; RORR: recovery of righting reflex; TH:
1160 tyrosine hydroxylase; icv.: intracerebroventricular; PS: photostimulation; *$p<0.05$;
1161 **$p<0.01$; ***$p<0.001$

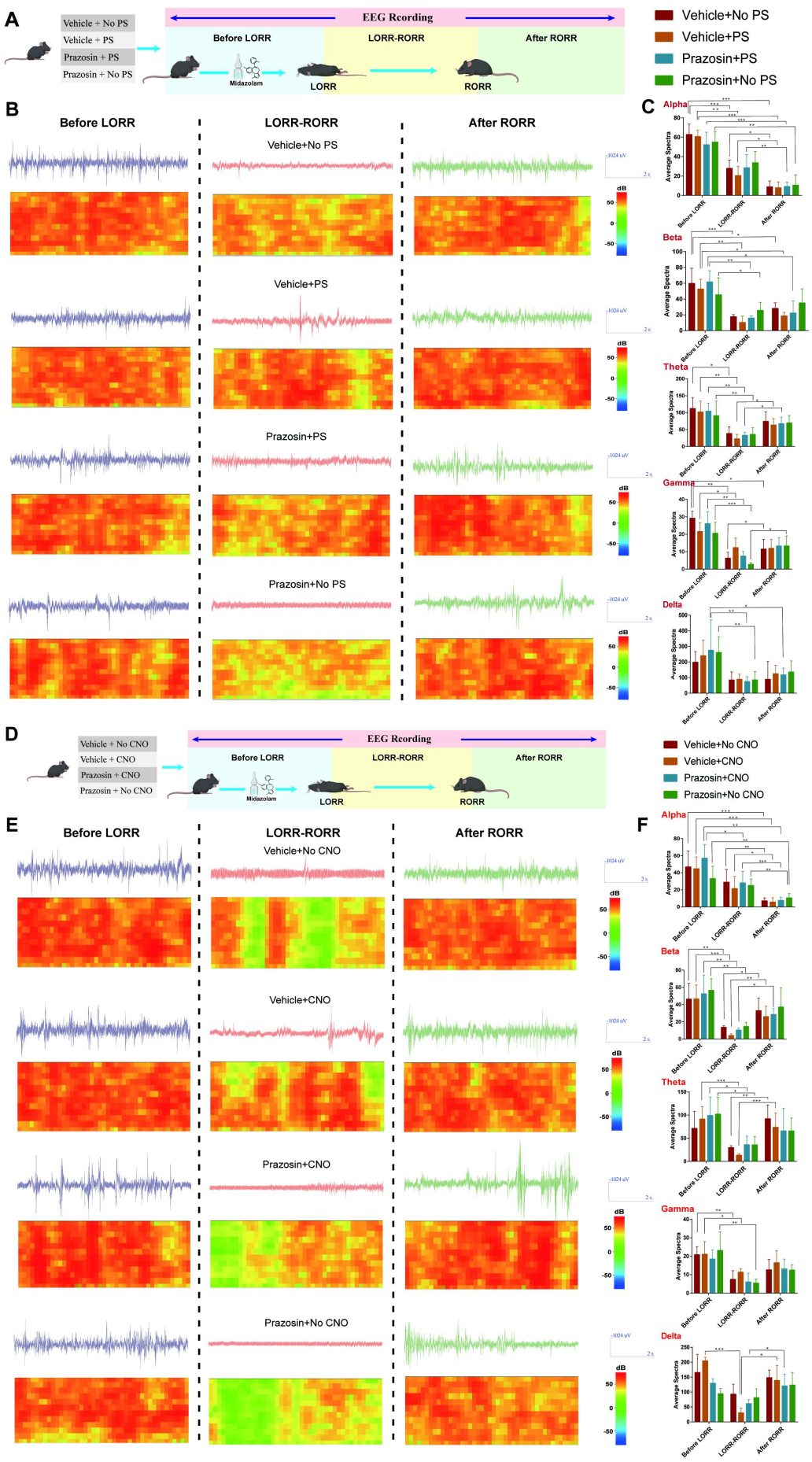
A
Vehicle + No PS
Vehicle + PS
Prazosin + PS
Prazosin + No PS
EEG Rcording
Before LORR
LORR-RORR
After RORR
Midazolam
LORR
RORR
Vehicle+No PS
Vehicle+PS
Prazosin+PS
Prazosin+No PS
B
Before LORR
LORR-RORR
After RORR
Vehicle+No PS
Vehicle+PS
Prazosin+PS
Prazosin+No PS
C
Alpha
Beta
Theta
Gamma
Delta
Average Spectra
D
Vehicle + No CNO
Vehicle + CNO
Prazosin + CNO
Prazosin + No CNO
Vehicle+No CNO
Vehicle+CNO
Prazosin+CNO
Prazosin+No CNO
E
F

1163 **Figure 7. Effect of ICV injection of α1-R antagonist and activation of LC^{NE}**
1164 **neurons on EEG activity**
1165 **(A, D)** Schematic diagram of EEG recording method.
1166 **(B)** EEG and spectrum of mice in vehicle+no PS, vehicle+PS, Prazosin+no PS, and
1167 Prazosin+PS at the *Before LORR*, *LORR-RORR*, and *After RORR* stages.
1168 (**C)** Alpha, Beta, Theta, Gamma, and Delta wave proportion of EEG in four groups of
1169 mice in different stages.
1170 **(E)** EEG and spectrum of mice in vehicle+no CNO, vehicle+ CNO, Prazosin+no
1171 CNO, and Prazosin+ CNO at the *Before LORR*, *LORR-RORR*, and *After RORR* stages.
1172 **(F)** Alpha, Beta, Theta, Gamma, and Delta wave proportion of EEG in four groups of
1173 mice in different stages.
1174 LC: locus coeruleus; LORR: loss of righting reflex; RORR: recovery of righting
1175 reflex; PS: photostimulation; *$p<0.05$; **$p<0.01$; ***$p<0.001$

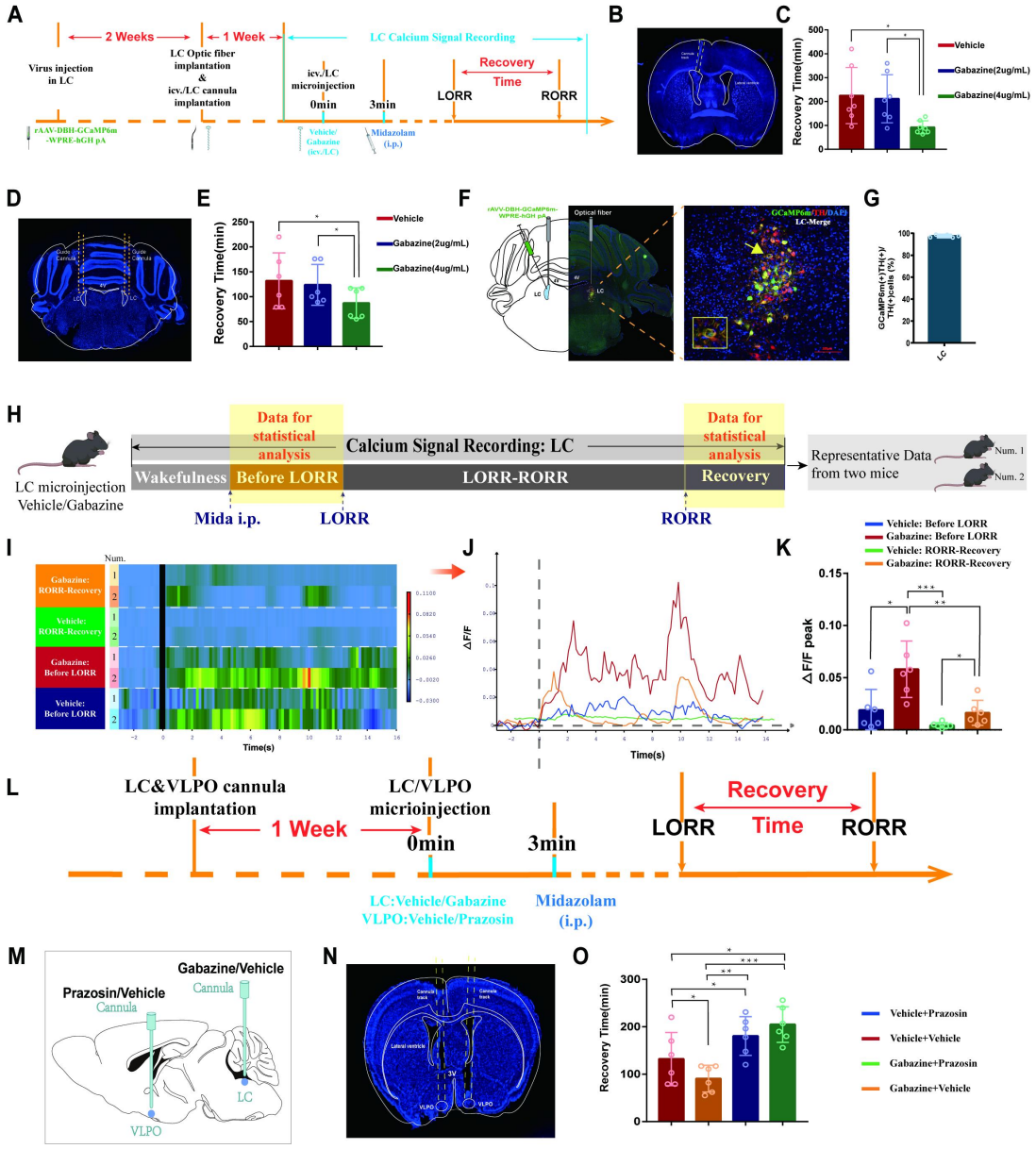

Figure 8. GABAA-R is an important mechanical binding site for midazolam in the LC

(A) Protocol for the fiber optic recording of calcium signals in the LC after intracerebroventricular injection or intra-LC microinjection of different doses of gabazine.

(B, D) A representative photomicrograph showing the tracks of cannulas implanted into the lateral ventricle and the bilateral LC.

(C, E) Results showed the effects of ICV injection or intra-LC microinjection of different doses of gabazine on the recovery time of midazolam.

(F) A representative photomicrograph showing the microinjection and optical fiber

locations and the co-expression of GCaMP6s and TH in the LC.

(G) Quantification of the percentage of GCaMP6m (+)/TH (+) colocalization in all TH (+) neurons in LC.

(H) Schematic diagram of the method of recording the calcium signal at the LC, and sources of statistical data.

(I) A heatmap of calcium signaling changes in bilateral LC^{NE} neurons induced by midazolam with or without intracerebroventricular injection of gabazine. (*Vehicle group*: n=2; *gabazine group*: n=2; Calcium signaling data from two representative mice per group. Calcium signaling information of each mouse in the stage *Before RORR* and *R-Recovery* were selected for presentation and further statistical analysis.) (The time points for midazolam injection and RORR in mice were respectively selected as time=0.The selected traces lasting for 20s was based on the length of a complete Ca2+ signal)

(J) A statistical diagram of calcium signaling changes in bilateral LC with or without intracerebroventricular injection of gabazine.

(K) The peak ΔF/F in the *Before RORR* and *RORR-Recovery* stages with or without intracerebroventricular injection of gabazine.

(L) Protocol for intra-LC microinjection of GABAA-R antagonist and intra-VLPO microinjection of α1-R antagonist.

(M) A schematic of the position of cannula implantation.

(N) A representative photomicrograph showing the tracks of cannulas implanted into the bilateral VLPO.

(O) Results showed the effects of intra-LC injection of gabazine and intra-VLPO injection of prazosin on the recovery time of midazolam.

LC: locus coeruleus; VLPO: ventrolateral preoptic nucleus; i.p.: intraperitoneal injection; LORR: loss of righting reflex; RORR: recovery of righting reflex; TH: tyrosine hydroxylase; icv.: intracerebroventricular; *$p<0.05$; **$p<0.01$; ***$p<0.001$

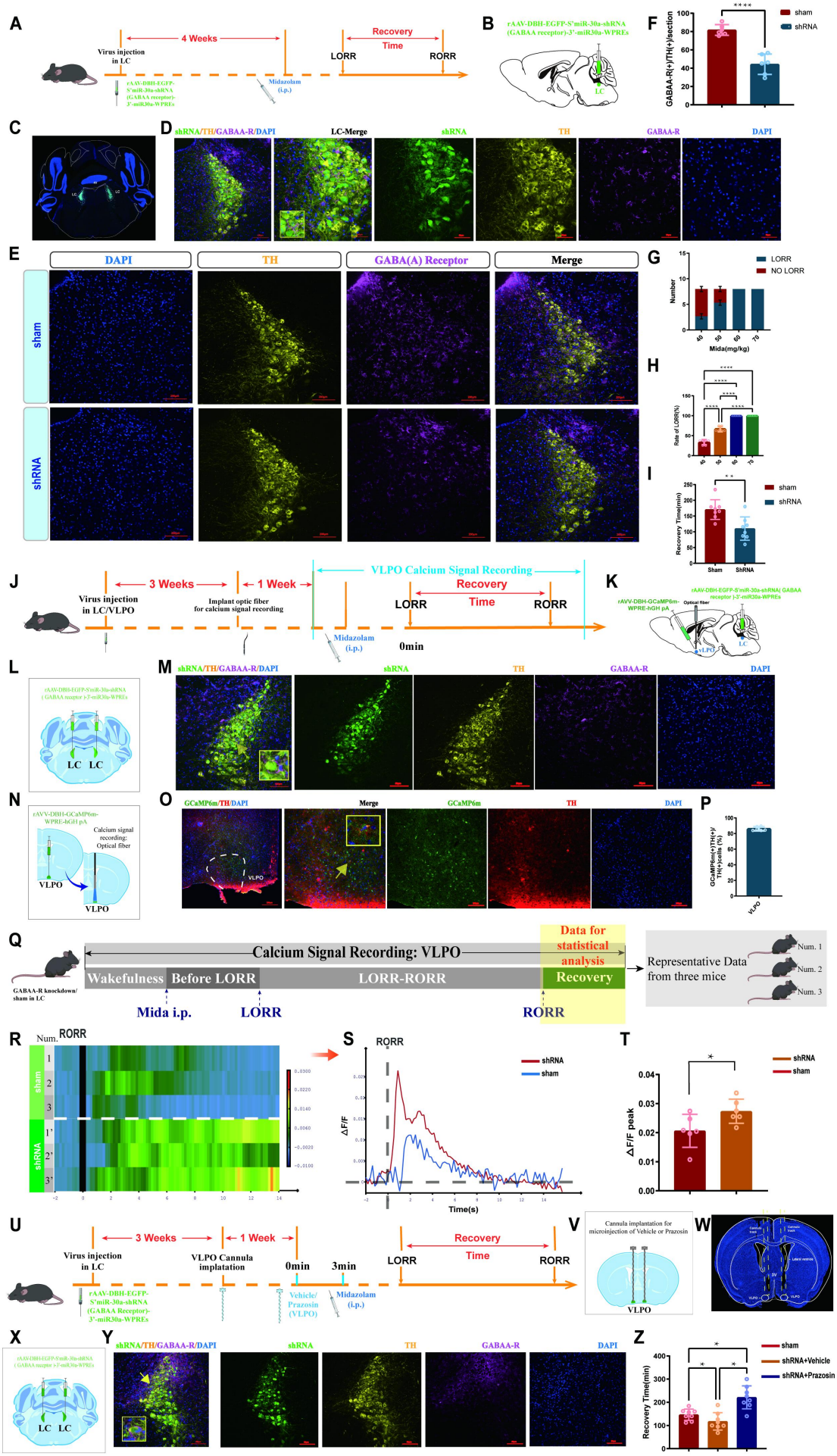
A
4 Weeks
Virus injection in LC
rAAV-DBH-EGFP-S'miR-30a-shRNA (GABAA receptor)-3'-miR30a-WPREs
Midazolam (i.p.)
Recovery Time
LORR
RORR
B
rAAV-DBH-EGFP-S'miR-30a-shRNA (GABAA receptor)-3'-miR30a-WPREs
LC
F
GABAA-R(+)/TH(+)/section
sham
shRNA
C
D
shRNA/TH/GABAA-R/DAPI
LC-Merge
shRNA
TH
GABAA-R
DAPI
E
DAPI
TH
GABA(A) Receptor
Merge
sham
shRNA
G
LORR
NO LORR
Number
Mida(mg/kg)
H
Rate of LORR(%)
I
Recovery Time(min)
Sham
ShRNA
J
3 Weeks
1 Week
Virus injection in LC/VLPO
Implant optic fiber for calcium signal recording
VLPO Calcium Signal Recording
Recovery Time
LORR
RORR
Midazolam (i.p.)
0min
K
rAAV-DBH-EGFP-S'miR-30a-shRNA(GABAA receptor)-3'-miR30a-WPREs
rAAV-DBH-GCaMP6m-WPRE-hGH pA
Optical fiber
VLPO
LC
L
rAAV-DBH-EGFP-S'miR-30a-shRNA (GABAA receptor)-3'-miR30a-WPREs
LC LC
M
shRNA/TH/GABAA-R/DAPI
shRNA
TH
GABAA-R
DAPI
N
rAVV-DBH-GCaMP6m-WPRE-hGH pA
Calcium signal recording: Optical fiber
VLPO
VLPO
O
GCaMP6m/TH/DAPI
Merge
GCaMP6m
TH
DAPI
VLPO
P
GCaMP6m(+)TH(+)/TH(+)cells (%)
VLPO
Q
GABAA-R knockdown/ sham in LC
Calcium Signal Recording: VLPO
Data for statistical analysis
Wakefulness
Before LORR
LORR-RORR
Recovery
Mida i.p.
LORR
RORR
Representative Data from three mice
Num. 1
Num. 2
Num. 3
R
Num.
RORR
sham
shRNA
S
RORR
shRNA
sham
ΔF/F
Time(s)
T
shRNA
sham
ΔF/F peak
U
3 Weeks
1 Week
Virus injection in LC
VLPO Cannula implatation
0min
3min
Recovery Time
LORR
RORR
rAAV-DBH-EGFP-S'miR-30a-shRNA (GABAA Receptor)-3'-miR30a-WPREs
Vehicle/ Prazosin (VLPO)
Midazolam (i.p.)
V
Cannula implantation for microinjection of Vehicle or Prazosin
VLPO
W
X
rAAV-DBH-EGFP-S'miR-30a-shRNA (GABAA receptor)-3'-miR30a-WPREs
LC LC
Y
shRNA/TH/GABAA-R/DAPI
shRNA
TH
GABAA-R
DAPI
Z
sham
shRNA+Vehicle
shRNA+Prazosin
Recovery Time(min)

1215 ~~reverses~~

1216 **Figure 9. GABA-ergic and NE-ergic systems interact with each other, co-regulate**
1217 **the recovery from midazolam**

1218 **(A)** Protocol for exploring the influence of knocking down the GABAA-R on the
1219 recovery time from midazolam.

1220 **(B-C)** Schematic diagram and the representative photomicrograph showing the
1221 position of virus injection.

1222 **(D)** A representative photomicrograph showing the co-expression of shRNA， TH，
1223 and GABAA-R in the LC.

1224 **(E)** Representative photomicrograph of the difference of GABAA-R expression in the
1225 LC after shRNA-mediated knockdown.

1226 **(F)** The quantification of GABAA-R (+)/TH (+) cells in the LC between the shRNA
1227 group and the sham group.

1228 **(G)** Number of LORR and no LORR induced by different doses of midazolam in
1229 GABAA-R knockdown mice.

1230 **(H)** Rate of LORR (%) in GABAA-R knockdown mice at different doses of
1231 midazolam.

1232 **(I)** The statistical bar shows shRNA-mediated GABAA-R knockdown effect on the
1233 recovery time from midazolam.

1234 **(J-K)** Protocol for exploring the calcium signals changes in the VLPO after knocking
1235 down the GABAA-R.

1236 **(L-M)** Schematic diagram and the representative photomicrograph showing the
1237 position of virus injection and the co-expression of shRNA， TH， and GABAA-R in
1238 the LC.

1239 **(N-O)** Schematic diagram of the brief process of calcium signal recording and the
1240 representative photomicrograph showing the co-expression of GCaP6m and TH in the
1241 VLPO.

1242 **(P)** Quantification of the percentage of GCaMP6m (+)/TH (+) colocalization in all
1243 TH (+) neurons in VLPO

1244 **(Q)** Schematic diagram of the method of recording the calcium signal at the VLPO,
1245 and sources of statistical data.

1246 **(R-S)** Heatmap and statistical diagram of calcium signaling changes in bilateral
1247 VLPO at the after RORR stage with or without knocking down GABAA-R on LC^{NE}

neurons. (Showing changes in calcium signaling during the RORR and the Recovery period; shRNA group, n=3; sham group, n=3) (The time points for RORR in mice were respectively selected as time=0.The selected traces lasting for 20s was based on the length of a complete Ca2+ signal)

(T) The peak ΔF/F in the VLPO with or without knocking down GABAA-R on LC^{NE} neurons.

(U) Protocol for exploring the effect of blocking α1-R in the VLPO and knocking down the GABAA-R in the LC on the recovery time from midazolam.

(V-W) Schematic diagram and the representative photomicrograph showing the positions of cannula implantation.

(X-Y) Schematic diagram and the representative photomicrograph showing the position of virus injection and the co-expression of shRNA， TH， and GABAA-R in the LC.

(Z) Results showed recovery time between sham, shRNA + Vehicle, and shRNA + Prazosin.

LC: locus coeruleus; VLPO: ventrolateral preoptic nucleus; i.p.: intraperitoneal injection; LORR: loss of righting reflex; RORR: recovery of righting reflex; TH: tyrosine hydroxylase; *p<0.05; ***p<0.001; ****p<0.0001

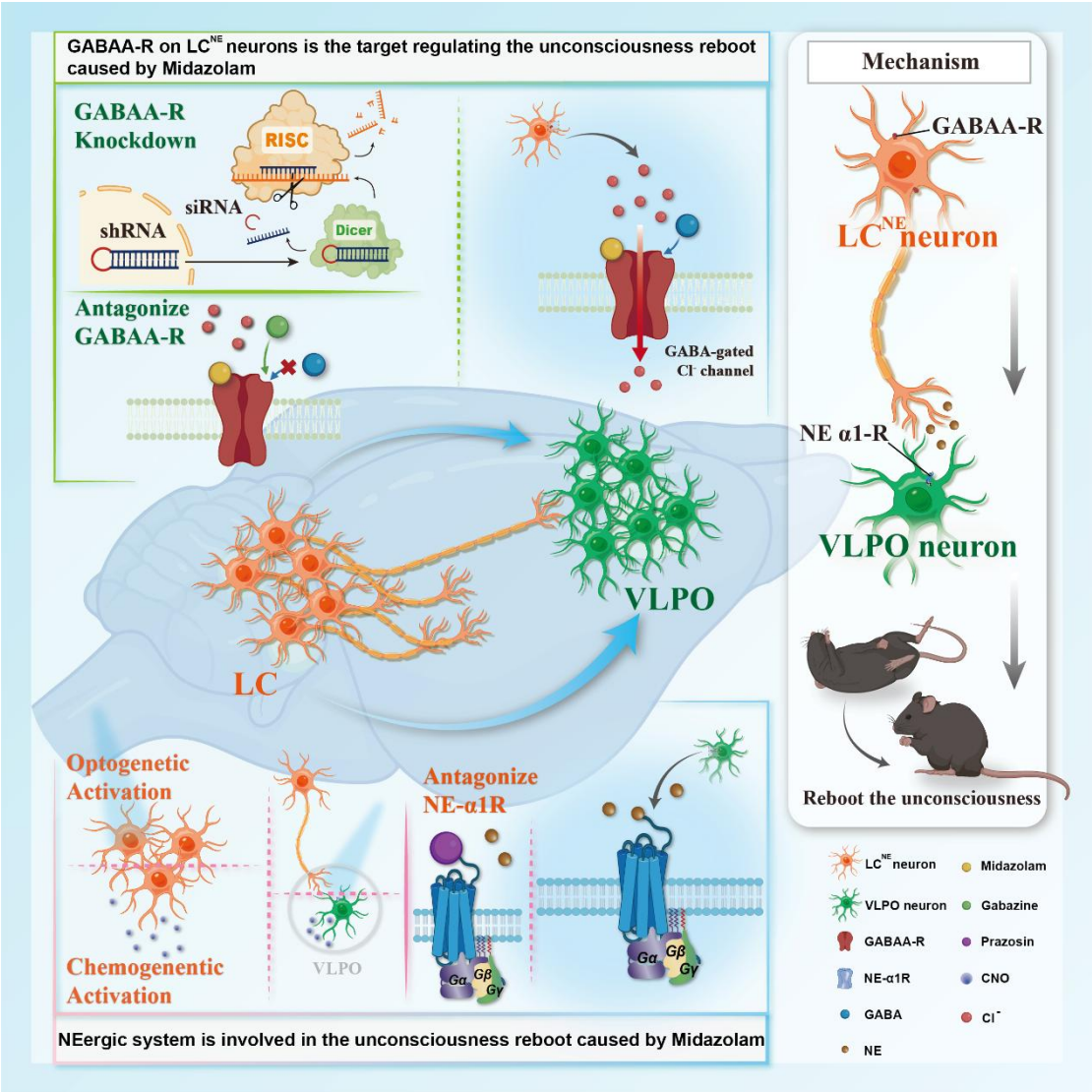

Figure 10. Summary of neural mechanism of rebooting the unconsciousness caused by midazolam

By using pharmacology, optogenetics, chemogenetics, fiber photometry, and gene knockdown, we revealed the role of locus coeruleus (LC)-ventrolateral preoptic nucleus (VLPO) noradrenergic neural circuit in regulating midazolam-induced altered consciousness. This effect was mediated by α1 adrenergic receptors. Moreover, gamma-aminobutyric acid receptor type A (GABAA-R) is a mechanistically important binding site in the LC for midazolam.

RISC: RNA-induced silencing complex; LC: locus coeruleus; VLPO: ventrolateral preoptic nucleus; NE: norepinephrine